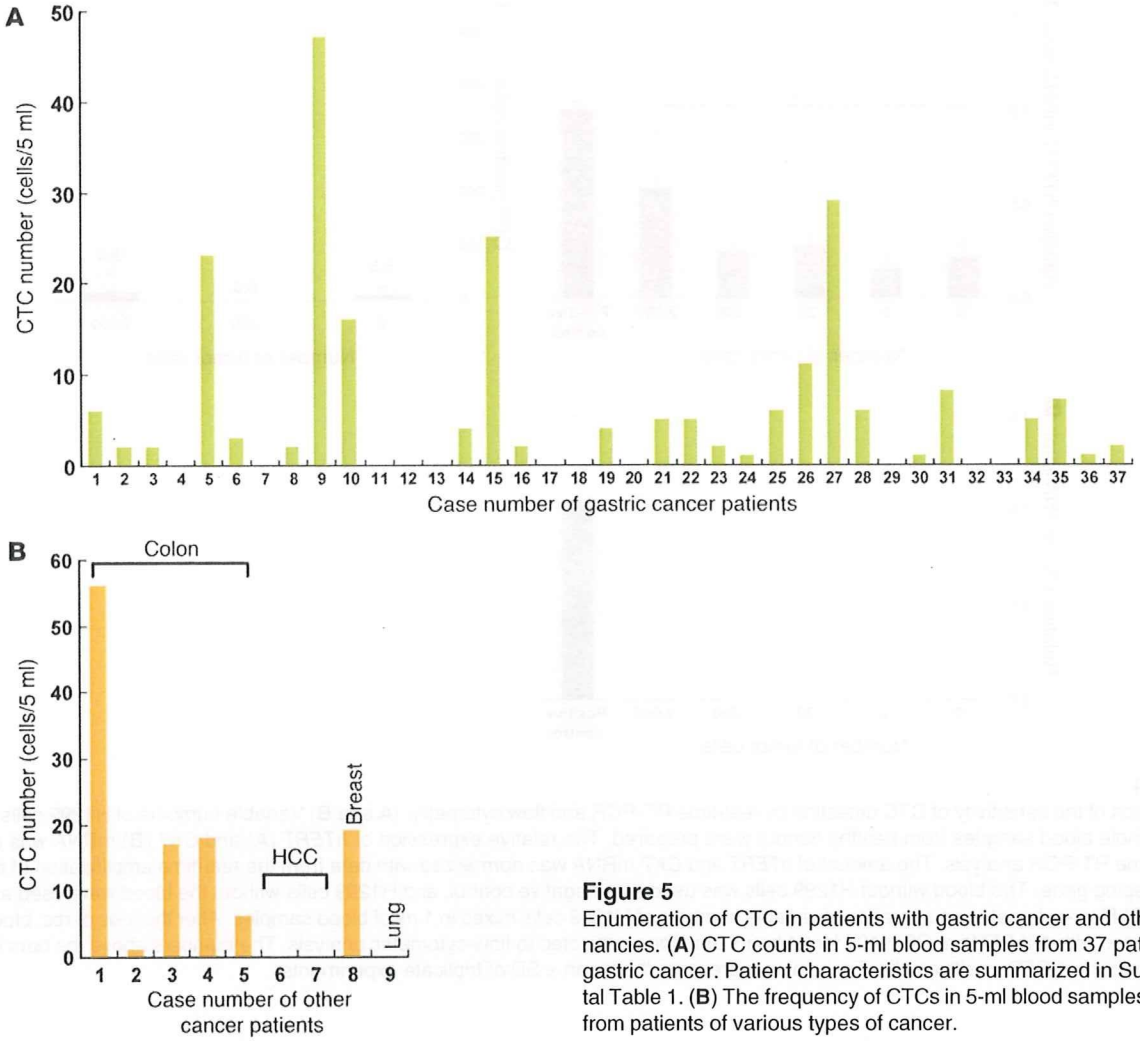

Figure 5
Enumeration of CTC in patients with gastric cancer and other malignancies. (**A**) CTC counts in 5-ml blood samples from 37 patients with gastric cancer. Patient characteristics are summarized in Supplemental Table 1. (**B**) The frequency of CTCs in 5-ml blood samples obtained from patients of various types of cancer.

state. In addition, our data demonstrated that neither quantitative RT-PCR for *hTERT* mRNA nor that for *CK7* mRNA could identify as many as 2,000 human tumor cells per 1 ml of blood without enrichment. Recently, Diehl et al. have reported that circulating tumor DNA is useful as a measure of tumor dynamics and that it can be beneficial for monitoring many types of human cancer (16). Although the system has the ability to quantify the level of circulating DNA and the sufficient sensitivity to detect very small amount of nucleic acids, it requires the identification of a somatic mutation in the individual tumor by sequencing of DNA. Our GFP-based fluorescence imaging can allow simple detection of target cancer cells, without any time-consuming steps, and it seems to be much more reliable and sensitive.

To date, various approaches have been also used to visually identify CTCs; however, the techniques employed to perform cell enrichment, immunohistochemical detection, and image analysis are complicated (17–19). Moreover, epithelial markers are currently used to detect CTCs; tumor cells, however, may lose their epithelial features during metastasis/dissemination or may not express these markers because of their heterogeneity (20). Indeed, the human non-small cell lung cancer cells that we used lack CK-19 expression, which is the marker most extensively studied for the detection of CTCs. The mechanism by which epithelial cells acquire the motile properties is epithelial-to-mesenchymal transition (EMT), a process that is currently popular for investigators of the onset of cancer cell migration, invasion, and metastatic dissemination (21, 22). EMT also promotes cytoskeletal rearrangement in tumor cells, which results in the downregulation of epithelial markers and upregulation of mesenchymal markers (22, 23). Nagrath et al. developed a unique microfluidic platform (CTC-chip) for CTC separation by using anti-epithelial cell adhesion molecule (EpCAM) antibody, and they demonstrated sensitive real-time monitoring of responses to cancer therapy with this technology (24); the loss of EpCAM expression, however, has been reported in metastatic and drug-resistant cancer cells (25). The multimarker assay may show slightly increased sensitivity for CTC detection over the single-marker method (26, 27); the procedures, however, are complicated. In contrast, telomerase is activated in most human cancers and is known to be associated with their malignant properties (28). Recent studies have reported that EMT can produce the cancer stem cell phenotype (29, 30). Since telomerase activity is one of the stem-cell properties (31), our system may be capable of detecting circulating cancer stem cells, even with EMT features, such as the loss and/or redistribution of the epithelial markers, that are

Table 1
CTC numbers classified by disease stage (as defined by the TNM classification system) and type

Cancer	Stage	GFP-positive cells (per 5 ml)					
		0	1–5	6–10	11–20	21–30	≥31
Gastric	I	5	5	2			1
Gastric	II		4			2	
Gastric	III	3	2	1			
Gastric	IV	3	4	1	2	1	
Colon	I				1		
Colon	II						
Colon	III			1	1		1
Colon	IV		1				
HCC	II	1					
HCC	III	1					
Breast	IV				1		
Lung	I	1					

responsible for metastasis. Moreover, as GFP-positive cells could be collected by flow-cytometric sorting (32), this technology might be applicable for molecular analysis of CTCs.

One of the crucial features that we believe to be unique of our approach is to use the virus with the self-proliferation potency. Although adenovirus-mediated transduction of the reporter genes into target cells is a common strategy in basic research, to the best of our knowledge, this is the first demonstration of ex vivo visualization of live CTCs, with a genetically engineered adenoviral agent, combined with an automated optical scan system for clinical studies. Infection efficiency of the adenoviral agent, which is derived from human adenovirus serotype 5, varies widely depending on the expression of Coxsackie-adenovirus receptor (CAR) (33). This might be one of the potential advantages of our system, because most of human hematopoietic cells are almost refractory to transduction by adenovirus vectors, due to the lack of CAR for virus binding (34). Therefore, when OBP-401 is used to detect CTCs in the peripheral blood, OBP-401 infection is limited in hematopoietic cells, including leukocytes. Moreover, OBP-401 replication is unlikely in normal hematopoietic cells, because of their low telomerase activity.

Our patient data demonstrate that enumeration of CTCs reflects the tumor burden, as the CTC counts decreased upon complete surgical removal of primary tumors. In addition, although the sample size is too small to perform a statistical analysis, 2 gastric cancer patients, who favorably responded to systemic chemotherapy, exhibited a gradual lowering of CTC counts in parallel with a decrease in the level of tumor markers, whereas a radiographically nonresponding patient had an increased CTC count. In contrast, the absolute number of CTCs did not correspond with tumor sizes or TNM stages in patients, and a small number of CTCs (0–4 cells in 5-ml samples) were detected in healthy normal volunteers (data not shown). These results suggest that it is more important to measure the change in CTC quantity, than to simply determine whether the value is below or above a disease-specific cutoff point; the CTC count was, however, mostly analyzed with this endpoint in clinical trials that used immunomagnetic-bead purification (3, 4, 17). Recently, Scher et al. have demonstrated that the use of CTC count as a continuous variable enables the prediction of survival in patients with castration-resistant prostate cancer (35). Although we cannot comment on the prognostic utility of CTC values in the absence of outcome data, our OBP-401–based method is at least useful as a measure of tumor dynamics. A larger series of clinical trials and longer follow-up studies are necessary to confirm the feasibility of this technology.

In conclusion, we developed an ex vivo GFP-based fluorescence imaging system that is very simple and suitable for accurate identification and enumeration of viable CTCs. This technology has the potential to allow physicians to assess the response to treatment as a relevant clinical parameter, especially in patients without elevated levels of tumor markers.

Methods

Cell culture. The human non-small cell lung cancer cell line H1299, the human tongue squamous carcinoma cell lines SCC-4 and SCC-9, the human gastric cancer cell line MKN45, the human colorectal cancer cell lines HT-29 and SW620, the human prostate cancer cell line PC-3, the human cervical adenocarcinoma cell line HeLa, and the human mammary gland adenocarcinoma cell line MCF-7 were cultured according to the specifications supplied by the vendor.

Virus. OBP-401 is a telomerase-specific replication-competent adenovirus variant, in which the hTERT promoter element drives the expression of the *E1A* and *E1B* genes linked with an internal ribosome entry site (IRES), and the *gfp* gene is inserted under the CMV promoter into the E3 region (7, 8, 10). The virus was purified by ultracentrifugation in cesium chloride step gradients, the titer was determined by a plaque-forming assay using 293 cells, and the virus sample was stored at -80°C.

Quantitative real-time RT-PCR analysis. Total RNA from cultured cells was obtained by using the RNeasy Mini Kit (Qiagen). The *hTERT* and *CK7* mRNA copy numbers were determined by real-time quantitative RT-PCR with a StepOnePlus system and TaqMan Gene Expression Assays (Applied Biosystems). Specific primers for hTERT (Hs00972650_m1), CK-7 (Hs00559840_m1), and GAPDH (Hs99999905_m1) were used (Applied Biosystems). PCR amplification began with a 20-second denaturation step at 95°C and then 40 cycles of denaturation at 95°C for 1 second and annealing/extension at 60°C for 20 seconds. Data analysis was performed using StepOne Software (Applied Biosystems). The *GAPDH* housekeeping gene was used as the reference gene for PCR normalization. The ratios normalized by dividing the value of H1299 cells were presented for each sample.

Fluorescence microplate reader. Cells were infected with OBP-401 at the indicated MOI values in a 96-well black-bottom culture plate and then further incubated for the indicated time periods. GFP fluorescence was measured by using a fluorescence microplate reader (DS Pharma Biomedical) with excitation/emission at 485 nm/528 nm. The GFP fluorescence was expressed relative to that of MCF-7 cells.

Time-lapse fluorescence microscopy. Cells were infected with OBP-401 at an MOI of 10 for 2 hours in vitro. Phase-contrast and fluorescent time-lapse recordings were obtained to concomitantly analyze cell morphology and GFP expression with an inverted microscope (Olympus) equipped with a heated stage and controlled CO_2 environment (37°C, 8.5% CO_2) (Tokai Hit). Images were taken every 10 minutes.

Sample preparation and automated optical imaging analysis. A simple 3-step method is used to detect viable human CTCs in the peripheral blood. Briefly, 5-ml blood samples were drawn into heparinized tubes and incubated with lysis buffer containing ammonium chloride (NH_4Cl) for 15 minutes to remove

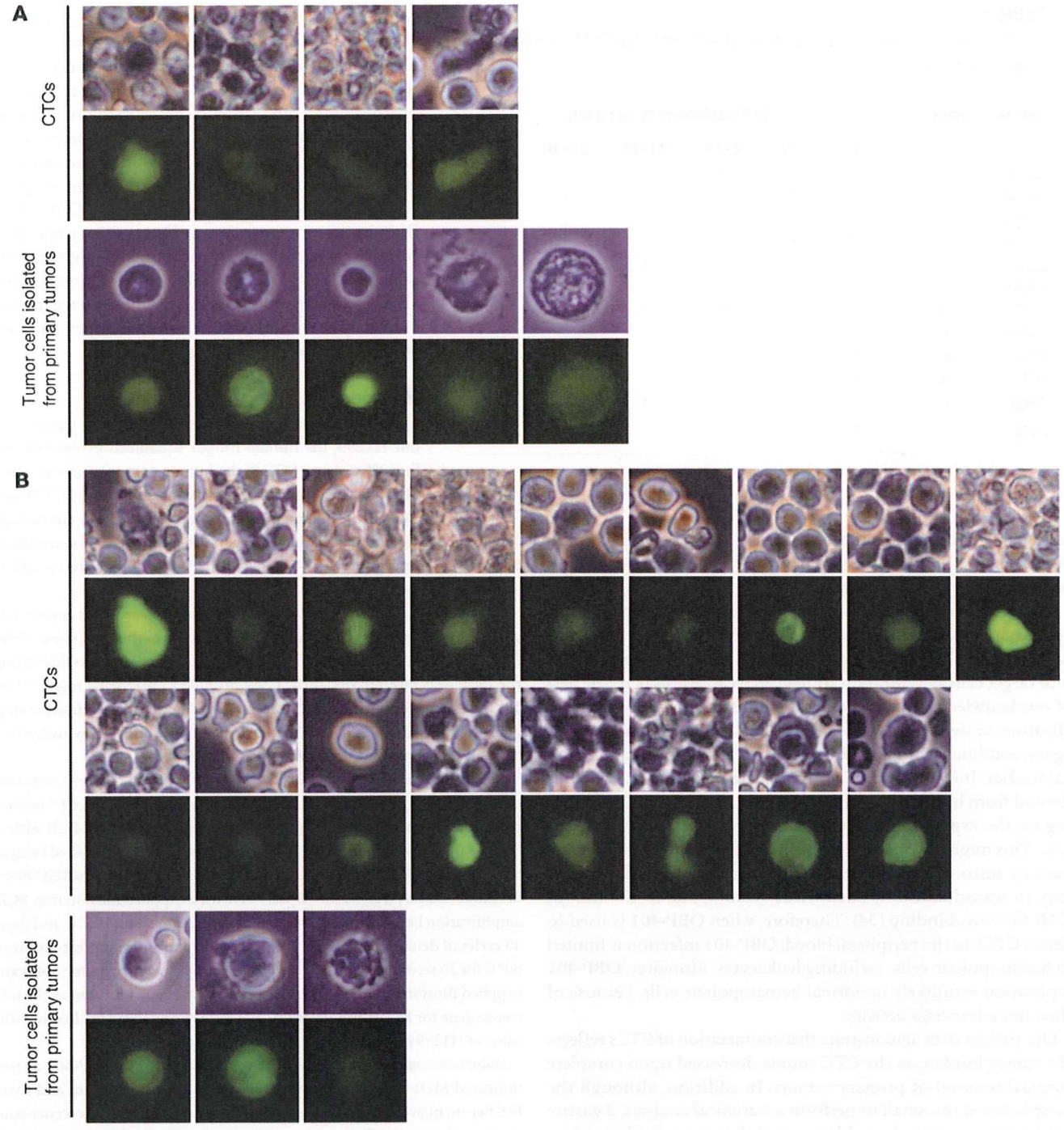

Figure 6
Images of GFP-positive cells obtained from the peripheral blood and the primary tumors. (**A**) CTCs were visualized by GFP expression among peripheral blood leukocytes in the blood sample obtained from a stage Ib gastric cancer patient (case 31). A single-cell suspension was also prepared from surgically removed primary tumor and exposed to OBP-401 at an MOI of 100 for 24 hours. (**B**) Primary tumor cells were also isolated from a patient with stage IIIa colon cancer (case 3) and infected with OBP-401 at an MOI of 100. Cell morphology of CTCs and primary tumor cells is shown by phase-contrast microscopy (first and third rows in **A** and first, third, and fifth rows in **B**), and GFP expression is shown by fluorescence microscopy (second and fourth rows in **A** and second, fourth, and sixth rows in **B**). Original magnification, ×600.

erythrocytes. After centrifugation, the cell pellets were mixed with 10^4 PFUs of OBP-401 and incubated at room temperature for another 24 hours. Following centrifugation, the cells were resuspended in 15 μl of PBS and then placed onto a slide under a coverslip. A motorized stage (Tokai Hit), mounted on a fluorescence microscope, serially captured segmented tile images in the area of the coverslip. The captured segmented tile images were joined together by MetaMorph 7.5, an image acquisition and analysis software (Molecular Devices), to create a large image of a 20-mm × 20-mm area. GFP signals could be

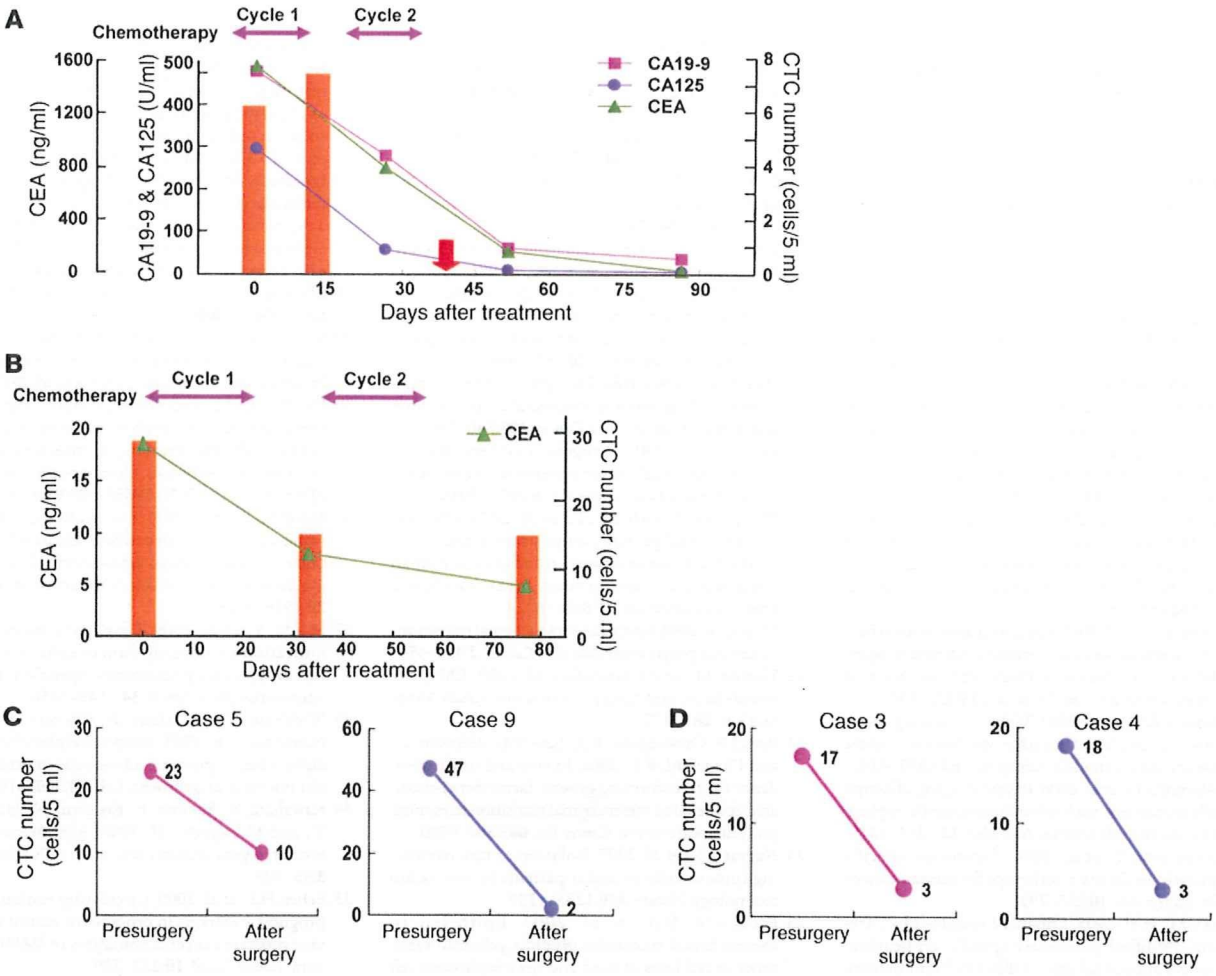

Figure 7

CTC dynamics at baseline and after treatment in patients with gastric or colon cancer. (**A**) Quantitation of CTCs in peripheral blood samples from an advanced gastric cancer patient (case 1) with multiple liver metastases who received 2 cycles of systemic chemotherapy. CTC counts at the indicated time points (orange bars) were plotted along with the levels of tumor markers CEA, CA19-9, and CA125. A decrease in the CTC number from 7 to 0 was observed 38 days after starting chemotherapy (red arrows). (**B**) The patient with recurrent gastric cancer at regional lymph nodes (case 27) was treated with 2 cycles of systemic chemotherapy. The CTC quantity (orange bars) and CEA level were well correlated over the course of treatment. (**C** and **D**) Changes in CTC numbers after surgery. CTC numbers were measured before and 4 weeks after surgical resection of primary tumors and regional lymph node dissection. (**C**) Two gastric cancer patients (cases 5 and 9) underwent a total gastrectomy and distal gastrectomy, respectively. (**D**) Low anterior resection was performed in 2 colorectal cancer patients (cases 3 and 4).

visualized easily in high-magnification images with a large field of view. The institutional review board at Okayama University Graduate School approved the study protocol, and all patients provided written informed consent.

Immunohistochemistry. Cells on the slides were fixed with 2% glutaraldehyde and washed 3 times with PBS. The slides were subsequently incubated with rhodamine-labeled anti-CK-7/8 antibody (CAM5.2; BD Biosciences) for 1 hour at 37°C. After washing 3 times with PBS, the slides were mounted with buffered glycerol for examination by fluorescence microscopy.

Tumor cell preparation. Primary solid tumors were surgically removed from patients with gastric cancer or other types of cancer. The tumor tissue was homogenized by mechanical mincing, and then the cell mixtures were passed through a cell strainer (BD Biosciences — Discovery Labware) and suspended as a single-cell suspension.

Statistics. We used the Student's 2-tailed *t* test to identify statistically significant differences between groups. Results are reported as mean ± SD. *P* values of less than 0.05 were considered statistically significant.

Acknowledgments

We thank Daiju Ichimaru and Hitoshi Kawamura for their helpful discussions. We also thank Tomoko Sueishi, Mitsuko Yokota, and Noriko Imagawa for their excellent technical supports. More importantly, we thank all participated patients for their courage and cooperation. This work was supported by Grants-in-Aid from the Ministry of Education, Science, and Culture, Japan and grants from the Ministry of Health and Welfare, Japan.

Received for publication January 16, 2009, and accepted in revised form July 1, 2009.

Address correspondence to: Toshiyoshi Fujiwara, Center for Gene and Cell Therapy, Okayama University Hospital, 2-5-1 Shikata-cho, Okayama 700-8558, Japan. Phone: 81-86-235-7997; Fax: 81-86-235-7884; E-mail: toshi_f@md.okayama-u.ac.jp.

1. Fidler, I.J. 1973. The relationship of embolic homogeneity, number, size and viability to the incidence of experimental metastasis. *Eur. J. Cancer.* **9**:223–227.
2. Liotta, L.A., Kleinerman, J., and Saidel, G.M. 1974. Quantitative relationships of intravascular tumor cells, tumor vessels, and pulmonary metastases following tumor implantation. *Cancer Res.* **34**:997–1004.
3. Cristofanilli, M., et al. 2004. Circulating tumor cells, disease progression, and survival in metastatic breast cancer. *N. Engl. J. Med.* **351**:781–791.
4. Cristofanilli, M., et al. 2005. Circulating tumor cells: a novel prognostic factor for newly diagnosed metastatic breast cancer. *J. Clin. Oncol.* **23**:1420–1430.
5. Hoffman, R.M. 2005. The multiple uses of fluorescent proteins to visualize cancer in vivo. *Nat. Rev. Cancer* **5**:796–806.
6. Umeoka, T., et al. 2004. Visualization of intrathoracically disseminated solid tumors in mice with optical imaging by telomerase-specific amplification of a transferred green fluorescent protein gene. *Cancer Res.* **64**:6259–6265.
7. Watanabe, T., et al. 2006. Histone deacetylase inhibitor FR901228 enhances the antitumor effect of telomerase-specific replication-selective adenoviral agent OBP-301 in human lung cancer cells. *Exp. Cell Res.* **312**:256–265.
8. Fujiwara, T., et al. 2006. Enhanced antitumor efficacy of telomerase-selective oncolytic adenoviral agent OBP-401 with docetaxel: Preclinical evaluation of chemovirotherapy. *Int. J. Cancer.* **119**:432–440.
9. Glinskii, A.B., et al. 2003. Viable circulating metastatic cells produced in orthotopic but not ectopic prostate cancer models. *Cancer Res.* **63**:4239–4243.
10. Kishimoto, H., et al. 2006. In vivo imaging of lymph node metastasis with telomerase-specific replication-selective adenovirus. *Nat. Med.* **12**:1213–1219.
11. Kawashima, T., et al. 2004. Telomerase-specific replication-selective virotherapy for human cancer. *Clin. Cancer Res.* **10**:285–292.
12. Taki, M., et al. 2005. Enhanced oncolysis by a tropism-modified telomerase-specific replication-selective adenoviral agent OBP-405 ('Telomelysin-RGD'). *Oncogene.* **24**:3130–3140.
13. Paterlini-Brechot, P., and Benali, N.L. 2007. Circulating tumor cells (CTC) detection: clinical impact and future directions. *Cancer Lett.* **253**:180–204.
14. Umetani, N., et al. 2006. Prediction of breast tumor progression by integrity of free circulating DNA in serum. *J. Clin. Oncol.* **24**:4270–4276.
15. Li, Y., et al. 2006. Serum circulating human mRNA profiling and its utility for oral cancer detection. *J. Clin. Oncol.* **24**:1754–1760.
16. Diehl, F., et al. 2008. Circulating mutant DNA to assess tumor dynamics. *Nat. Med.* **14**:985–990.
17. Allard, W.J., et al. 2004. Tumor cells circulate in the peripheral blood of all major carcinomas but not in healthy subjects or patients with nonmalignant diseases. *Clin. Cancer Res.* **10**:6897–6904.
18. Half, E., et al. 2004. HER-2 receptor expression, localization, and activation in colorectal cancer cell lines and human tumors. *Int. J. Cancer.* **108**:540–548.
19. Fehm, T., et al. 2002. Cytogenetic evidence that circulating epithelial cells in patients with carcinoma are malignant. *Clin. Cancer Res.* **8**:2073–2084.
20. Willipinski-Stapelfeldt, B., et al. 2005. Changes in cytoskeletal protein composition indicative of an epithelial-mesenchymal transition in human micrometastatic and primary breast carcinoma cells. *Clin. Cancer Res.* **11**:8006–8014.
21. Thiery, J.P. 2002. Epithelial-mesenchymal transitions in tumour progression. *Nat. Rev. Cancer.* **2**:442–454.
22. Yilmaz, M., and Christofori, G. 2009. EMT, the cytoskeleton, and cancer cell invasion. *Cancer Metastasis Rev.* **28**:15–33.
23. Rees, J.R., Onwuegbusi, B.A., Save, V.E., Alderson, D., and Fitzgerald, R.C. 2006. In vivo and in vitro evidence for transforming growth factor-beta1-mediated epithelial to mesenchymal transition in esophageal adenocarcinoma. *Cancer Res.* **66**:9583–9590.
24. Nagrath, S., et al. 2007. Isolation of rare circulating tumour cells in cancer patients by microchip technology. *Nature.* **450**:1235–1239.
25. Frederick, B.A., et al. 2007. Epithelial to mesenchymal transition predicts gefitinib resistance in cell lines of head and neck squamous cell carcinoma and non-small cell lung carcinoma. *Mol. Cancer Ther.* **6**:1683–1691.
26. Xi, L., et al. 2007. Optimal markers for real-time quantitative reverse transcription PCR detection of circulating tumor cells from melanoma, breast, colon, esophageal, head and neck, and lung cancers. *Clin. Chem.* **53**:1206–1215.
27. Ignatiadis, M., et al. 2008. Prognostic value of the molecular detection of circulating tumor cells using a multimarker reverse transcription-PCR assay for cytokeratin 19, mammaglobin A, and HER2 in early breast cancer. *Clin. Cancer Res.* **14**:2593–2600.
28. Blackburn, E.H. 2000. Telomere states and cell fates. *Nature.* **408**:53–56.
29. Santisteban, M., et al. 2009. Immune-induced epithelial to mesenchymal transition in vivo generates breast cancer stem cells. *Cancer Res.* **69**:2887–2895.
30. Dembinski, J.L., and Krauss, S. 2009. Characterization and functional analysis of a slow cycling stem cell-like subpopulation in pancreas adenocarcinoma. *Clin. Exp. Metastasis.* Online publication ahead of print. doi:10.1007/s10585-009-9260-0.
31. Maurelli, R., et al. 2006. Inactivation of p16INK4a (inhibitor of cyclin-dependent kinase 4A) immortalizes primary human keratinocytes by maintaining cells in the stem cell compartment. *FASEB J.* **20**:1516–1518.
32. Maida, Y., et al. 2009. Diagnostic potential and limitation of imaging cancer cells in cytological samples using telomerase-specific replicative adenovirus. *Int. J. Oncol.* **34**:1549–1556.
33. Wickham, T.J., Mathias, P., Cheresh, D.A., and Nemerow, G.R. 1993. Integrins alpha v beta 3 and alpha v beta 5 promote adenovirus internalization but not virus attachment. *Cell.* **73**:309–319.
34. Kawabata, K., Sakurai, F., Koizumi, N., Hayakawa, T., and Mizuguchi, H. 2006. Adenovirus vector-mediated gene transfer into stem cells. *Mol. Pharm.* **3**:95–103.
35. Scher, H.I., et al. 2009. Circulating tumour cells as prognostic markers in progressive, castration-resistant prostate cancer: a reanalysis of IMMC38 trial data. *Lancet Oncol.* **10**:233–239.

Selective metastatic tumor labeling with green fluorescent protein and killing by systemic administration of telomerase-dependent adenoviruses

Hiroyuki Kishimoto,[1,2,3] Yasuo Urata,[5] Noriaki Tanaka,[3] Toshiyoshi Fujiwara,[3,4] and Robert M. Hoffman[1,2]

[1]AntiCancer, Inc.; [2]Department of Surgery, University of California, San Diego, California; [3]Division of Surgical Oncology, Department of Surgery, Okayama University Graduate School of Medicine, Dentistry and Pharmaceutical Sciences; [4]Center for Gene and Cell Therapy, Okayama University Hospital, Okayama, Japan; and [5]Oncolys BioPharma, Inc., Tokyo, Japan

Abstract

We previously constructed telomerase-dependent, replication-selective adenoviruses OBP-301 (Telomelysin) and OBP-401 [Telomelysin-green fluorescent protein (GFP); TelomeScan], the replication of which is regulated by the human telomerase reverse transcriptase promoter. By intratumoral injection, these viruses could replicate within the primary tumor and subsequent lymph node metastasis. The aim of the present study was to evaluate the possibility of systemic administration of these telomerase-dependent adenoviruses. We assessed the antitumor efficacy of OBP-301 and the ability of OBP-401 to deliver GFP in hepatocellular carcinoma (HCC) and metastatic colon cancer nude mouse models. We showed that i.v. administration of OBP-301 significantly inhibited colon cancer liver metastases and orthotopically implanted HCC. Further, we showed that OBP-401 could visualize liver metastases by tumor-specific expression of the *GFP* gene after portal venous or i.v. administration. Thus, systemic administration of these adenoviral vectors should have clinical potential to treat and detect liver metastasis and HCC. [Mol Cancer Ther 2009;8(11):3001–8]

Introduction

Primary and metastatic liver tumors are a common cause of death throughout the world. Hepatocellular carcinoma (HCC), the most common primary liver tumor, is the fifth most common malignancy and the third most frequent cause of cancer death worldwide (1, 2). HCC often metastasizes widely, and distant metastatic sites include lung, bone, adrenals, and brain. The 5-year survival rates of these patients are usually in the range of 16% to 25% (3). Colorectal cancer is also one of the most common tumors worldwide. The liver is the most preferential site for metastasis of colorectal cancer and over half of these patients die from their metastatic liver diseases (4). Therefore, management of the liver metastases is a key factor for colorectal cancer prognosis.

Liver resection is the only potentially curative treatment option available for patients with primary and metastatic liver tumors (5, 6). However, because only a minority of patients with colorectal liver metastases or HCC are candidates for surgery (7–10), new therapeutic agents and innovative approaches for tumor detection are desired.

We previously constructed two conditionally replicating type 5 adenoviruses OBP-301 (Telomelysin) and OBP-401 [Telomelysin-green fluorescent protein (GFP); TelomeScan]. The replication of these viruses is regulated by the human telomerase reverse transcriptase (hTERT) promoter (11–15). hTERT is the catalytic subunit of telomerase, which is highly active in cancer cells but quiescent in most normal somatic cells (16). Therefore, these adenoviruses have tumor-specific replication regulated by the hTERT transcriptional activity. OBP-301 has shown a strong anticancer efficacy in a variety of tumors *in vitro* and *in vivo* (11, 12, 17–19). We also reported that OBP-401 can replicate in and label cancer cells with GFP *in vitro* and *in vivo* and thereby enables imaging of tumor cells by GFP fluorescence *in vivo* (15). Tumor specificity is conferred by selective replication of OBP-401 in the cancer cells. Replication of the virus, and therefore production of GFP, depends on the tumor-specific expression of telomerase. In those studies, however, the virus was administered locally such as by intratumoral injection or administration into a body cavity (thoracic or abdominal cavity). The efficacy of these viruses, when administered systemically, has not been evaluated.

In the present study, we examined the feasibility of systemic administration of OBP-301 and OBP-401 to colorectal liver metastases and to orthotopic HCC tumor in nude mice models, focusing on the antitumor efficacy of OBP-301 and the ability of OBP-401 to selectively induce *GFP* gene expression in cancer cells.

Materials and Methods

Recombinant Adenovirus

We previously constructed OBP-301, in which the hTERT promoter element drives the expression of the *E1A* and *E1B* genes linked with an internal ribosome entry site (11–14).

Received 6/22/09; revised 8/17/09; accepted 9/1/09; published OnlineFirst 11/3/09.

Grant support: National Cancer Institute grant CA132242.

The costs of publication of this article were defrayed in part by the payment of page charges. This article must therefore be hereby marked *advertisement* in accordance with 18 U.S.C. Section 1734 solely to indicate this fact.

Requests for reprints: Robert M. Hoffman, AntiCancer, Inc., San Diego, CA 92111. Phone: 858-654-2555, Fax: 858-268-4175. E-mail: all@anticancer.com

Copyright © 2009 American Association for Cancer Research.

doi:10.1158/1535-7163.MCT-09-0556

OBP-401, was derived from OBP-301 and also contains the *GFP* gene under the control of the cytomegalovirus promoter, was also constructed previously (15, 20). These viruses were purified by ultracentrifugation in cesium chloride step gradients. Their titers were determined by a plaque-forming assay using 293 cells. The viruses were stored at −80°C.

Cell Culture

The human colorectal cancer cell line HCT-116 and the human HCC cell lines Hep3B and HepG2 were obtained from the American Type Culture Collection. The cells were cultured in RPMI 1640 (Irvine Scientific) supplemented with 10% fetal bovine serum.

GFP Gene Transduction of Cancer Cells

For *GFP* gene transduction of cancer cells, 20% confluent HCT-116 or Hep3B cells were incubated with a 1:1 precipitated mixture of retroviral supernatants of the PT67 GFP-expressing packaging cells and RPMI 1640 containing 10% fetal bovine serum for 72 h. Fresh medium was replenished at this time. Tumor cells were harvested by trypsin/EDTA 72 h post-transduction and subcultured at a ratio of 1:15 into selective medium containing 200 μg/mL G418. The level of G418 was increased up to 800 μg/mL in a stepwise manner. GFP-expressing cancer cells were isolated with cloning cylinders (Bel-Art Products) using trypsin/EDTA and amplified by conventional culture methods in the absence of selective agent.

Animal Experiments

Athymic nude mice were kept in a barrier facility under HEPA filtration and fed with autoclaved laboratory rodent diet (Teklad LM-485; Western Research Products). All animal studies were conducted in accordance with the principles and procedures outlined in the NIH Guide for the Care and Use of Laboratory Animals under assurance no. A3873-1. All animal procedures were done under anesthesia using s.c. administration of a ketamine mixture (10 μL ketamine HCl, 7.6 μL xylazine, 2.4 μL acepromazine maleate, and 10 μL PBS).

Experimental Liver Metastasis Model of Human Colon Cancer

To generate a liver metastasis model, unlabeled HCT-116 or HCT-116-GFP human colon cancer cells were injected

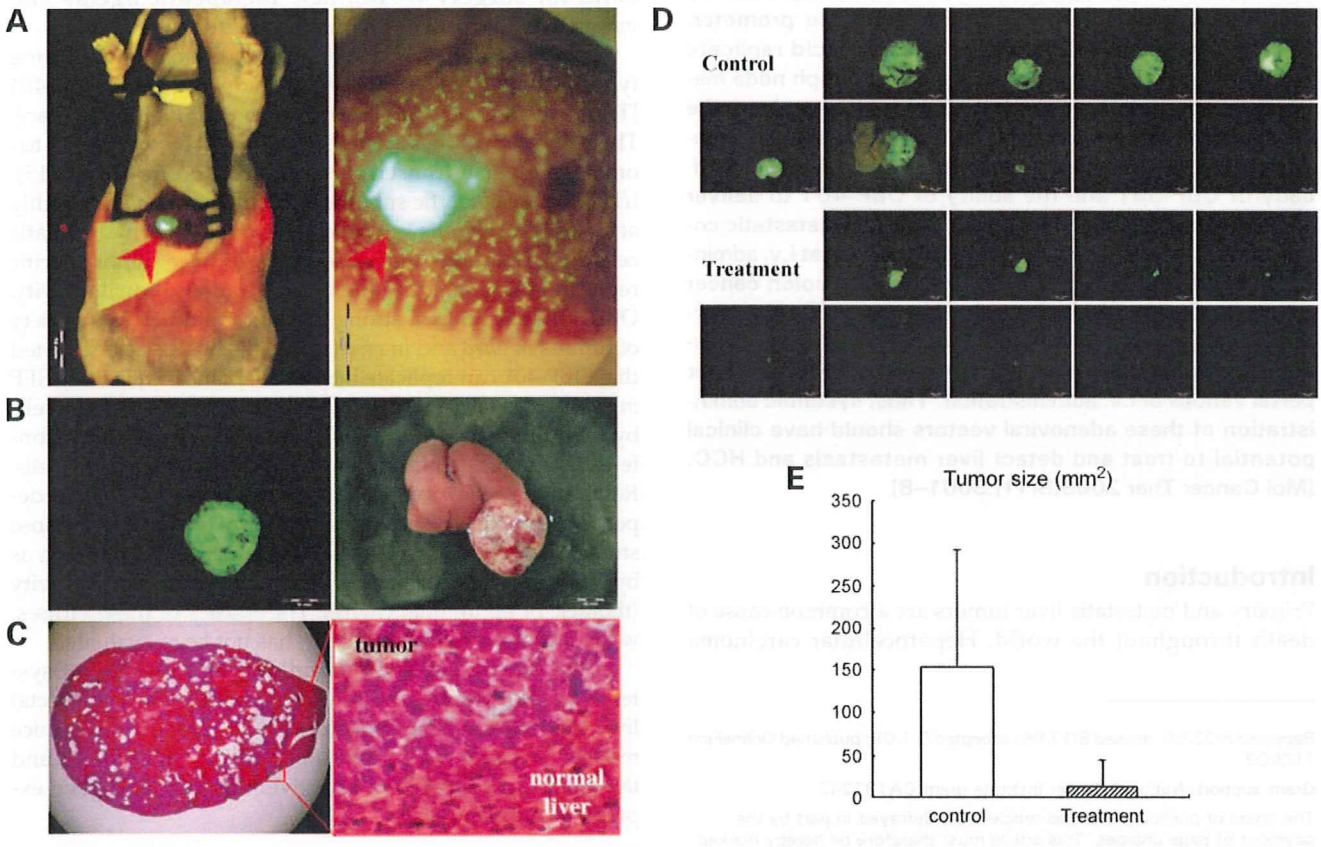

Figure 1. Efficacy of systemic OBP-301 administration on orthotopic HCC. **A,** Hep3B-GFP cells were subserosally injected into the left lobe of the liver (*red arrow*) to generate an orthotopic liver tumor model (*left*). Some cells could be seen accumulating in the terminal portal veins near the bleb of the injected site (*right*). **B,** macroscopic appearance of Hep3B-GFP liver tumor 8 wk after inoculation. *Left,* fluorescence detection; *right,* bright-field observation. **C,** H&E staining of Hep3B-GFP liver tumor section. *Left,* magnification, ×10; *right,* detail of the boxed region. Magnification, ×400. **D,** macroscopic appearance of liver. Livers were excised 8 wk after Hep3B-GFP cells injection. OBP-301 or PBS were i.v. injected biweekly starting from 2 wk after tumor cell inoculation. Excised livers were photographed under fluorescence. **E,** quantitative analysis of the tumor size (fluorescent area) of control and OBP-301–treated mice ($P < 0.01$).

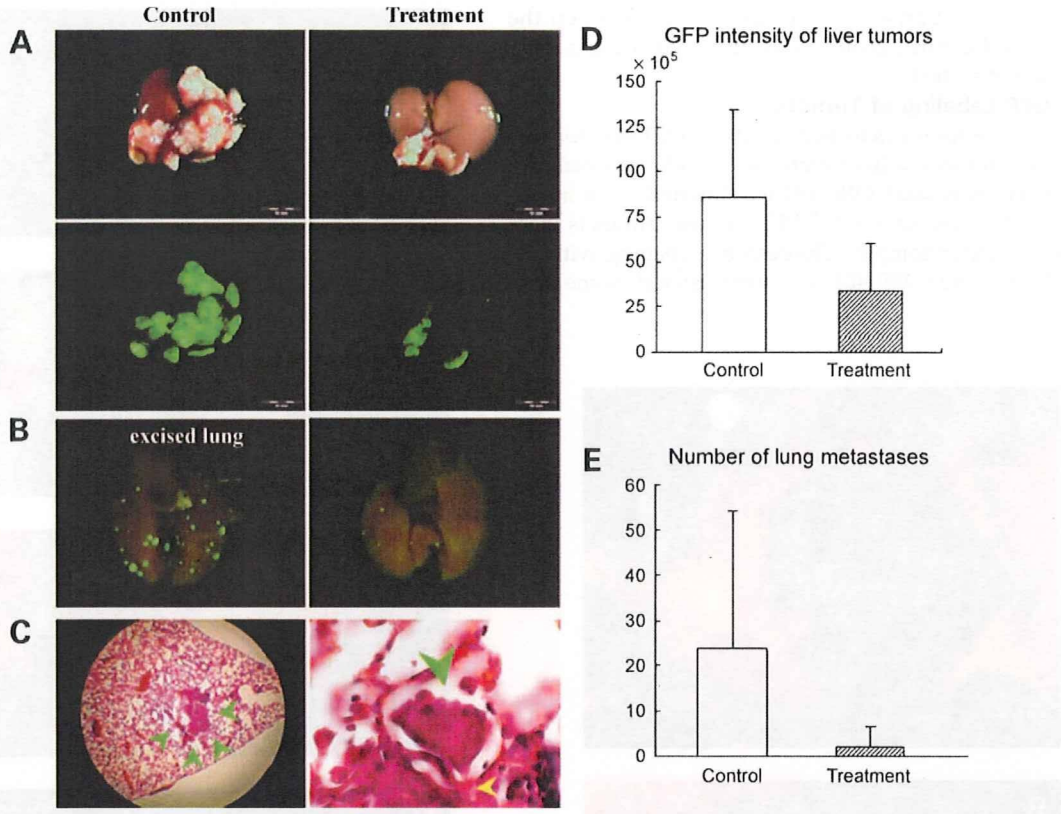

Figure 2. Systemic OBP-301 therapy of colon cancer liver metastases. **A,** macroscopic appearance of livers. HCT-116-GFP cells were injected into the spleen of nude mice, and the liver was excised 6 wk later. OBP-301 or PBS were i.v. injected 5 d after tumor cell inoculation. Excised livers were photographed under bright light (*top*). Fluorescence imaging showed GFP expression signals on the HCT-116-GFP liver metastasis (*bottom*). **B,** macroscopic appearance of lungs. Lung metastatic foci were detected with GFP fluorescence. *Left,* control; *right,* OBP-301 treatment significantly suppressed lung metastasis. **C,** H&E staining of lung metastasis in control mouse (*green arrow*). *Left,* magnification, ×40; *right,* protrusion of tumor (*green arrow*) into the adjacent alveoli through the Kohn's pore (*yellow arrow*). Magnification, ×400. **D,** quantitative analysis of the total GFP intensity in the liver of control and OBP-301–treated mice ($P < 0.05$). **E,** quantitative analysis of the number of lung metastases of control and OBP-301–treated mice ($P < 0.05$).

at a density of 2×10^6 in 50 μL Matrigel (BD Biosciences) into the spleen of nude mice through a 28-gauge needle at laparotomy.

Orthotopic Liver Tumor Model of HCC

An orthotopic liver tumor model with human HCC was made with unlabeled Hep3B or Hep3B-GFP human HCC cells. Unlabeled Hep3B or Hep3B-GFP cells (5.0×10^6 in 10 μL Matrigel) were subserosally injected into the left lobe of the liver through a 28-gauge needle at laparotomy. Unlabeled HepG2 cells, cells (3×10^6 in 50 μL Matrigel) were injected into the spleen of nude mice through a 28-gauge needle at laparotomy.

Antitumor Efficacy Studies

To assess the antitumor efficacy of i.v. administration of OBP-301 against liver metastases of the colorectal cancer, OBP-301 was injected once systemically into the tail vein at a dose of 5×10^8 plaque forming units (PFU)/100 μL 5 days after HCT-116-GFP cells were injected into the spleen. Control mice were injected with 100 μL PBS in an identical manner ($n = 9$ mice per group). Six weeks after tumor cell inoculation (5 weeks after treatment), fluorescence imaging was done using an Olympus OV100 Imaging System. GFP fluorescent intensity of the liver metastases and the number of lung metastases were determined. To obtain GFP intensity, exposure conditions were maintained constant at 30 ms to keep the data comparable. GFP intensity was quantified and presented in the units of SUM green intensity using Cell software (Olympus-Biosystems). The experimental data are presented as mean ± SD. Comparison of the GFP intensity and the number of lung metastases between the treatment and control groups were analyzed using a two-tailed Student's *t* test.

The antitumor efficacy of i.v. administration of OBP-301 was also assessed in an orthotopic liver tumor model of HCC. OBP-301 was i.v. injected biweekly (5×10^8 PFU/2 weeks for 6 weeks) starting from 2 weeks after Hep3B-GFP cells were injected into the liver. Control mice were injected with 100 μL PBS in an identical manner ($n = 9$ mice per group). All animals were examined 8 weeks after cancer cell inoculation (2 weeks after last treatment). Development of tumor growth and response to OBP-301 treatment were evaluated by the fluorescent area of the liver tumor calculated by Cell software using GFP images obtained with the Olympus OV100. The experimental data are presented as

mean ± SD. Comparison of the tumor area between the treatment and control groups was analyzed using a two-tailed Student's *t* test.

Viral GFP Labeling of Tumors

To assess the tumor detection ability of OBP-401 for metastatic liver tumors, a liver metastasis model of unlabeled HCT-116 cells was used. OBP-401 was injected i.v. or intrasplenically at a dose of 1×10^8 PFU/mouse. Animals were examined at laparotomy by fluorescence imaging with the OV100 5 days after OBP-401 was administered. Some mice had a second-look observation 1 week after the first open examination.

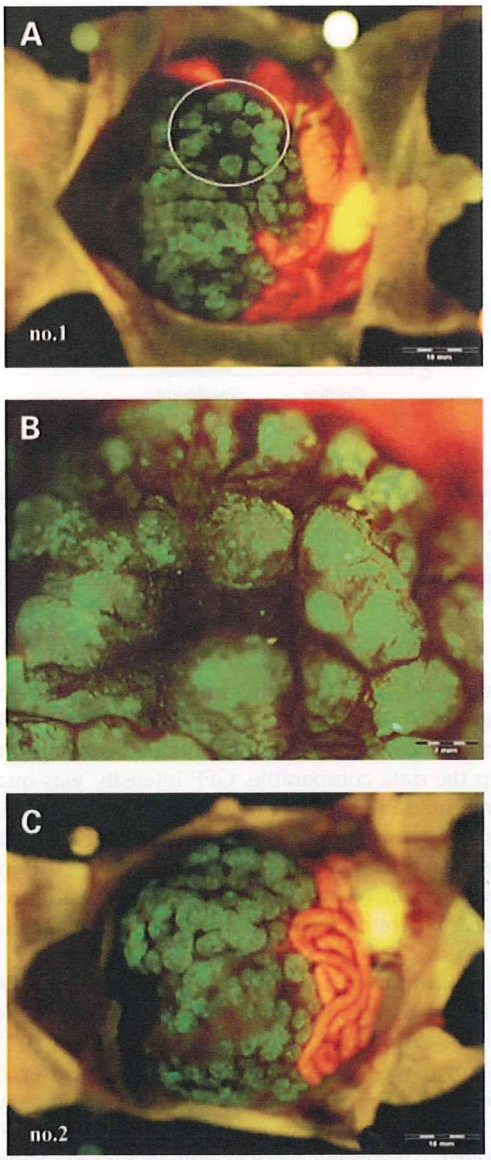

Figure 3. Portal venous delivery of OBP-401 selectively labeled multiple colon cancer liver metastases. **A,** gross appearance of the abdominal cavity (mouse no. 1). Five days after splenic injection of OBP-401, HCT-116 liver metastases were visualized by GFP fluorescence. **B,** higher magnification of the liver surface indicated by the *white circle* in **A**. **C,** liver metastases were visualized by GFP fluorescence in mouse no. 2.

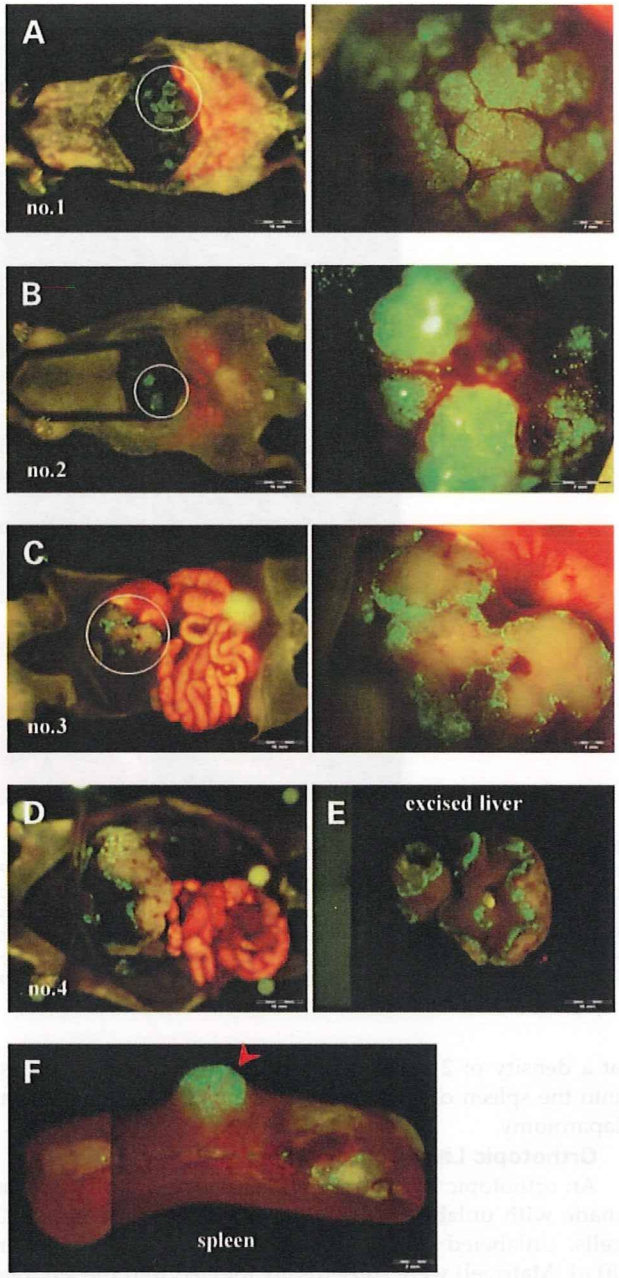

Figure 4. Selective GFP labeling of multiple liver metastases of human colon cancer by i.v. injection of OBP-401. **A** to **C,** 5 d after i.v. injection with OBP-401, HCT-116 liver metastases were visualized by GFP fluorescence (mouse nos. 1-3; *left*). Higher magnification of the liver metastasis indicated by a white circle (*right*). **D,** gross appearance of the abdominal cavity (mouse no. 4). **E,** macroscopic appearance of excised liver in mouse no. 4. The margin of the liver metastasis was visualized by GFP fluorescence. **F,** macroscopic appearance of spleen. Tumor development in the spleen was also visualized by GFP fluorescence 5 d after OBP-401 treatment (*red arrow*).

To assess the tumor detection ability of OBP-401 in the orthotopic liver tumor model, unlabeled Hep3B cells were

used. OBP-401 was injected systemically into the tail vein at a dose of 1×10^8 PFU/mouse 2 weeks after tumor cell inoculation. Animals were examined at laparotomy by fluorescence imaging with the OV100 5 days after OBP-401 was administered. Some mice had a second-look observation 4 weeks after i.v. injection of OBP-401.

Fluorescence Optical Imaging and Processing

The Olympus OV100 Imaging System containing an MT-20 light source was used. High-resolution images are captured directly on a PC (Fujitsu Siemens), and images are analyzed with the use of Cell software (Olympus-Biosystems).

Results and Discussion

Liver Metastasis Model of Human Colon Cancer

Intrasplenic inoculation of nude mice with unlabeled HCT-116 or HCT-116-GFP human colon cancer cells led to multiple experimental metastases in the liver within 14 days. With HCT-116-GFP, spleen tumors and lung metastasis could also be observed by fluorescence imaging at 6 weeks after cancer cell implantation.

Orthotopic Liver Tumor Model of HCC

When unlabeled Hep3B or Hep3B-GFP human HCC cells were subserosally injected into the liver of nude mice (Fig. 1A), a small tumor mass (~2 mm) was often observed on the liver surface by 2 weeks after cancer cell inoculation. Hep3B liver tumors usually grew only in the injected lobe and rarely spread to other lobes (Fig. 1B). These tumors showed abundant tumor blood vessels, indicating a rich blood supply for the tumor, which reflects HCC in human patients (Fig. 1C).

Unlabeled HepG2 cells were also inoculated in the spleen of nude mice with the same technique used in the experimental colorectal liver metastasis model. Two weeks after tumor cell inoculation, multiple HepG2 tumors were observed on the liver surface.

Inhibition of Experimental Colon Cancer Metastasis by OBP-301

OBP-301 was i.v. injected at a dose of 5×10^8 PFU/mouse 5 days after HCT-116-GFP inoculation in the spleen. At 6 weeks after HCT-116-GFP colon cancer cell inoculation, 100% of the control animals developed liver tumors, and tumors in the spleen developed in 40% of control animals. Treatment with OBP-301 caused a significant inhibition in liver metastasis growth ($P < 0.05$; Fig. 2A and D). Additionally, OBP-301–treated animals showed a reduced number of lung metastases colonies compared with controls ($P < 0.05$; Fig. 2B and E). These results show that systemic dosing of OBP-301 has significant antitumor activity against experimental colon cancer liver metastasis. In contrast to the experimental liver metastasis, OBP-301 did not have an apparent effect on the spleen tumors. The lack of effect of OBP-301 on the spleen tumors may be because of their very small size, which made differences difficult to discern.

Inhibition of Orthotopic HCC by OBP-301

To evaluate the antitumor efficacy of OBP-301 on HCC tumors, the orthotopic liver tumor model of Hep3B-GFP was used.

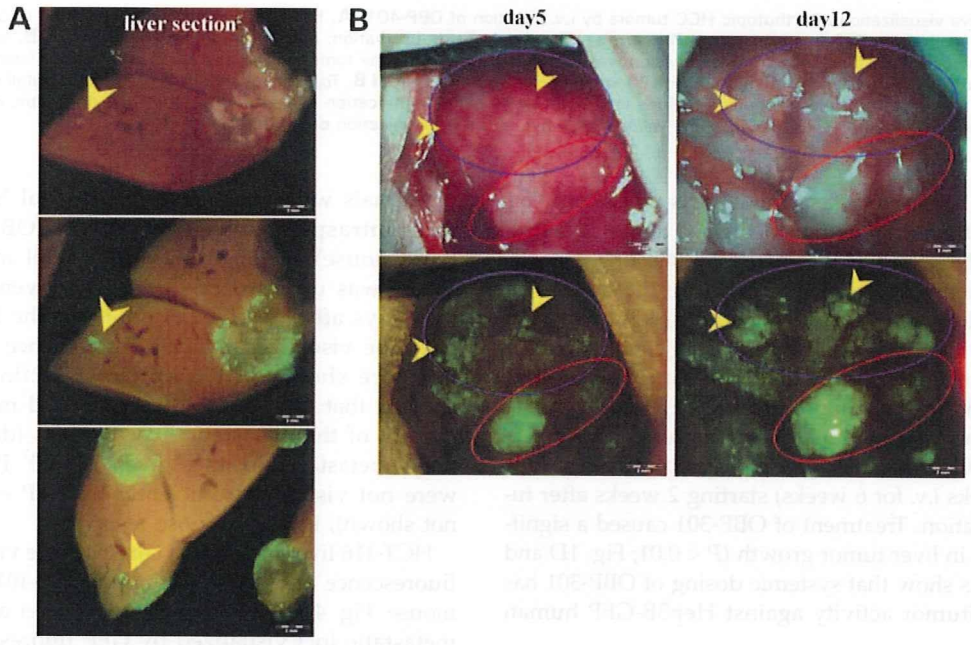

Figure 5. Early metastatic liver tumors not otherwise clearly visible could be visualized after i.v. injection of OBP-401. **A,** cross-sections of liver. GFP expression was mainly located at the periphery of the liver metastases. Tiny metastatic foci not otherwise clearly visible were visualized by GFP fluorescence after i.v. injection of OBP-401 (*yellow arrow*). **B,** 5 d after i.v. injection of OBP-401, HCT-116 liver metastases were visualized by GFP fluorescence (*red circle*). There were areas in the liver, which had GFP expression but seemed to be tumor-free in bright light (*blue circle*). Seven days later, metastases could be visualized by bright light as well as GFP fluorescence (*yellow arrows*), showing the power of OBP-401 to label very early, otherwise invisible metastases with GFP.

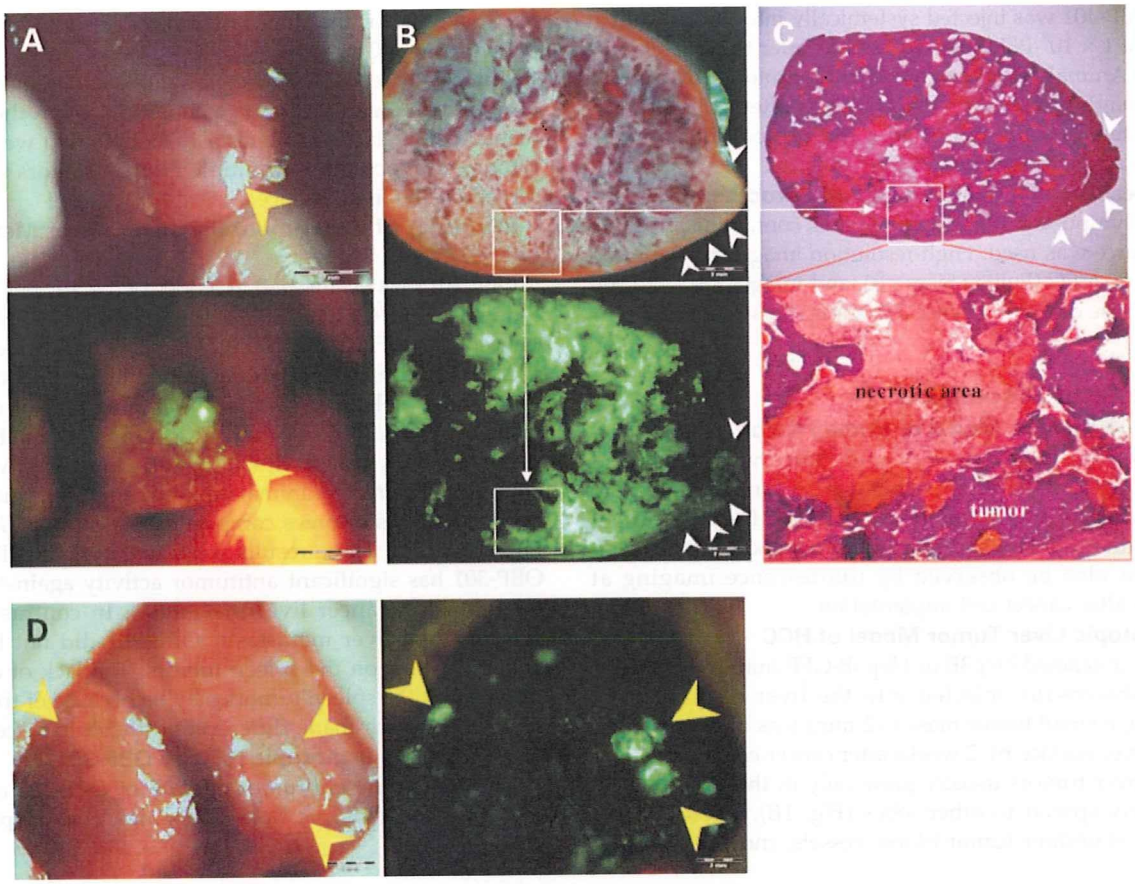

Figure 6. Selective visualization of orthotopic HCC tumors by i.v. injection of OBP-401. **A,** 5 d after systemic administration of OBP-401, orthotopic Hep3B HCC was visualized by GFP fluorescence (*yellow arrow*). *Top,* bright-field observation; *bottom,* fluorescence detection. **B,** cross-section of liver tumor 4 wk after i.v. injection of OBP-401. GFP expression was selectively detected in the tumor. *White arrow* indicates normal liver tissue. *Top,* bright-field observation; *bottom,* fluorescence detection. **C,** H&E section of Hep3B liver tumor of **B**. *Top,* magnification, ×10; *bottom,* detail of the boxed region. Magnification, ×40. Boxes refer to corresponding regions in **B** and **C** with high magnification in **B** and **C** (*bottom*). **D,** orthotopic HepG2 HCC tumors (*yellow arrows*) were visualized by GFP fluorescence (*yellow arrows*) 4 wk after i.v. injection of OBP-401.

The colorectal liver metastasis model was made by delivering cells into the portal vein as described above, whereas the orthotopic HCC model was made by injecting cells directly into the hepatic parenchyma, where at the early stage of tumor development most cells were thought to locate outside of the blood vessels. Thus, i.v. injected OBP-301 could target cancer cells more effectively in the colorectal liver metastasis model than in the HCC model. In the HCC model, therefore, we increased the number of injections of OBP-301, which was administered biweekly (5×10^8 PFU/2 weeks i.v. for 6 weeks) starting 2 weeks after tumor cell inoculation. Treatment of OBP-301 caused a significant inhibition in liver tumor growth ($P < 0.01$; Fig. 1D and E). These results show that systemic dosing of OBP-301 has significant antitumor activity against Hep3B-GFP human HCC tumors.

Selective Visualization of Colorectal Liver Metastases by OBP-401 Delivery of the GFP Gene

To assess the tumor detection ability of OBP-401 for colorectal liver metastases, OBP-401 was administrated to mice by portal venous delivery or systemic delivery using the tail vein.

Animals with HCT-116 experimental liver metastases were intrasplenically injected with OBP-401 (1×10^8 PFU/mouse) 12 days after tumor cell inoculation. The spleen was used to access the portal venous circulation. Five days after injection of OBP-401, the liver metastases could be visualized by GFP fluorescence. Representative mice are shown in Fig. 3. Cross-sections of the liver showed that GFP fluorescence occurred mainly at the periphery of the metastatic liver nodules (data not shown). Liver metastases in mice given 1×10^7 PFU of OBP-401 were not visualized efficiently by GFP expression (data not shown), indicating dose response.

HCT-116 liver metastases could also be visualized by GFP fluorescence after i.v. injection of OBP-401 (1×10^8 PFU/mouse; Fig. 4). Cross-sections of the liver also showed tiny metastatic foci visualized by GFP fluorescence (Fig. 5A). Moreover, a second-look observation done 1 week after the first laparotomy showed that early metastatic liver tumors, not clearly visible under bright light, had been visualized with GFP fluorescence after i.v. injection of OBP-401 at as early as day 5, indicating the possibility of early

detection of metastatic disease (Fig. 5B). When injected with more than 2×10^8 PFU of OBP-401, mice often showed GFP fluorescence in normal tissues such as liver, lung, spleen, and thoracic duct (data not shown). Theses results suggest that colorectal liver metastases can be visualized by GFP fluorescence both by portal venous and i.v. administration of OBP-401.

Selective Visualization of Orthotopic HCC by OBP-401

Five days after injection of OBP-401 (1×10^8 PFU/mouse) into the tail vein, HCC liver tumors were visualized by GFP fluorescence (Fig. 6A). Cross-sections of the liver at 4 weeks after i.v. injection of OBP-401 showed that GFP expression was in the cancer cells and not in normal cells (Fig. 6B and C). Small liver tumor nodules were also visualized by GFP fluorescence after i.v. OBP-401 administration (Fig. 6D). Thus, we showed that HCC liver tumors could be selectively visualized by GFP fluorescence after i.v. injection of OBP-401.

Many studies have shown that the majority of malignant human tumors tested express hTERT. OBP-301 and OBP-401 specifically replicate in tumors due to hTERT expression in tumors (11, 12, 17–19). In previous studies, OBP-301 and OBP-401 were administered locally, such as by intratumoral or intrapleural administration. The present report shows the systemic efficacy of OBP-301 and OBP-401 to selectively replicate in and kill and label primary and metastatic liver tumors after i.v. administration. Closely related virus constructs will be compared with OBP-301 and OBP-401 in the future.

Our laboratory pioneered the use of fluorescent proteins to visualize cancer cells *in vivo*. Cancer cells genetically labeled by fluorescent proteins have increased the possibility and sensitivity to observe progression of cancer cells in live animals (21). To evaluate antitumor efficacy of i.v. administration of OBP-301 against primary and metastatic liver tumors, we used GFP-expressing human cancer cell lines. We showed that i.v. administration of OBP-301 resulted in a significant reduction in experimental liver and pulmonary metastases in a colorectal liver metastases model and effectively inhibited tumor formation and growth in an orthotopic HCC model. OBP-401 has less but still significant cytotoxic effects compared with OBP-301 (22). In fact, a significant inhibition of tumor growth by intratumoral injection of OBP-401 was confirmed *in vivo* in our previous study (20). However, OBP-401 at the tumor-selective labeling dose used in this i.v. injection study could not inhibit tumor growth effectively.

The imaging strategy using OBP-401 has a potential of being available in humans as a navigation system in the surgical treatment of malignancy. During surgery, tumors that would be difficult to detect by direct visual detection could be positively identified with GFP fluorescence using a handheld excitation light and appropriate filter goggles as we have shown previously in mice (23–25). Employment of a fluorescence surgical microscope would enable visualization of the GFP-expressing microscopic leading edge of the tumor and allow accurate resection with sufficient margins.

As for toxicity of OBP-301 and OBP-401, only when injected with 5×10^8 PFU OBP-301 for the first time, a few mice showed lethargy but fully recovered within 1 h. None of the mice treated with OBP-301 or OBP-401 at the doses used in this study showed significant adverse effects during the observation period or histopathologic changes in the liver at the time of sacrifice. In the near future, the safety of OBP-301 will be confirmed in a phase I clinical trial, which is currently under way (26).

Our studies suggest the clinical potential of OBP-301 and OBP-401.

Disclosure of Potential Conflicts of Interest

No potential conflicts of interest were disclosed.

References

1. Bruix J, Hessheimer AJ, Forner A, Boix L, Vilana R, Llovet JM. New aspects of diagnosis and therapy of hepatocellular carcinoma. Oncogene 2006;25:3848–56.
2. Okuda K. Hepatocellular carcinoma. J Hepatol 2000;32:225–37.
3. Takayasu K, Muramatsu Y, Moriyama N, et al. Clinical and radiologic assessments of the results of hepatectomy for small hepatocellular carcinoma and therapeutic arterial embolization for postoperative recurrence. Cancer 1989;64:1848–52.
4. Koshariya M, Jagad RB, Kawamoto J, et al. An update and our experience with metastatic liver disease. Hepato-gastroenterology 2007;54:2232–9.
5. Kavolius J, Fong Y, Blumgart LH. Surgical resection of metastatic liver tumors. Surg Oncol Clin N Am 1996;5:337–52.
6. Chouillard E, Cherqui D, Tayar C, Brunetti F, Fagniez PL. Anatomical bi- and trisegmentectomies as alternatives to extensive liver resections. Ann Surg 2003;238:29–34.
7. Jiao LR, Hansen PD, Havlik R, Mitry RR, Pignatelli M, Habib N. Clinical short-term results of radiofrequency ablation in primary and secondary liver tumors. Am J Surg 1999;177:303–6.
8. Khatri VP, Petrelli NJ, Belghiti J. Extending the frontiers of surgical therapy for hepatic colorectal metastases: is there a limit? J Clin Oncol 2005; 23:8490–9.
9. Adam R. Chemotherapy and surgery: new perspectives on the treatment of unresectable liver metastases. Ann Oncol 2003;14 Suppl 2:ii13–6.
10. Bismuth H, Adam R, Lévi F, et al. Resection of nonresectable liver metastases from colorectal cancer after neoadjuvant chemotherapy. Ann Surg 1996;224:509–20, discussion 520–2.
11. Kawashima T, Kagawa S, Kobayashi N, et al. Telomerase-specific replication-selective virotherapy for human cancer. Clin Cancer Res 2004;10: 285–92.
12. Taki M, Kagawa S, Nishizaki M, et al. Enhanced oncolysis by a tropism-modified telomerase-specific replication-selective adenoviral agent OBP-405 ('telomelysin-RGD'). Oncogene 2005;24:3130–40.
13. Umeoka T, Kawashima T, Kagawa S, et al. Visualization of intrathoracically disseminated solid tumors in mice with optical imaging by telomerase-specific amplification of a transferred green fluorescent protein gene. Cancer Res 2004;64:6259–65.
14. Hashimoto Y, Watanabe Y, Shirakiya Y, et al. Establishment of biological and pharmacokinetic assays of telomerase-specific replication-selective adenovirus. Cancer Sci 2008;99:385–90.
15. Kishimoto H, Kojima T, Watanabe Y, et al. *In vivo* imaging of lymph node metastasis with telomerase-specific replication-selective adenovirus. Nat Med 2006;12:1213–9.
16. Takakura M, Kyo S, Kanaya T, et al. Cloning of human telomerase catalytic subunit (hTERT) gene promoter and identification of proximal core promoter sequences essential for transcriptional activation in immortalized and cancer cells. Cancer Res 1999;59:551–7.
17. Watanabe T, Hioki M, Fujiwara T, et al. Histone deacetylase inhibitor FR901228 enhances the antitumor effect of telomerase-specific

replication-selective adenoviral agent OBP-301 in human lung cancer cells. Exp Cell Res 2006;312:256–65.

18. Hioki M, Kagawa S, Fujiwara T, et al. Combination of oncolytic adenovirotherapy and Bax gene therapy in human cancer xenografted models. Potential merits and hurdles for combination therapy. Int J Cancer 2008;122:2628–33.

19. Huang P, Watanabe M, Kaku H, et al. Direct and distant antitumor effects of a telomerase-selective oncolytic adenoviral agent, OBP-301, in a mouse prostate cancer model. Cancer Gene Ther 2008;15:315–22.

20. Fujiwara T, Kagawa S, Kishimoto H, et al. Enhanced antitumor efficacy of telomerase-selective oncolytic adenoviral agent OBP-401 with docetaxel: preclinical evaluation of chemovirotherapy. Int J Cancer 2006;119:432–40.

21. Hoffman RM. The multiple uses of fluorescent proteins to visualize cancer *in vivo*. Nat Rev Cancer 2005;5:796–806.

22. Kyo S, Takakura M, Fujiwara T, Inoue M. Understanding and exploiting hTERT promoter regulation for diagnosis and treatment of human cancers. Cancer Sci 2008;99:1528–38.

23. Yang M, Luiken G, Baranov E, Hoffman RM. Facile whole-body imaging of internal fluorescent tumors in mice with an LED flashlight. Biotechniques 2005;39:170–2.

24. Kishimoto H, Zhao M, Hayashi K, et al. *In vivo* internal tumor illumination by telomerase-dependent adenoviral GFP for precise surgical navigation. Proc Natl Acad Sci U S A 2009;106:14514–7.

25. Jasni BR. Green surgery. Science 2009;325:1321.

26. Fujiwara T, Tanaka N, Numunaitis JJ, et al. Phase I trial of intratumoral administration of OBP-301, a novel telomerase-specific oncolytic virus, in patients with advanced solid cancer. Evaluation of biodistribution and immune response. J Clin Oncol 2008;26:3572.

© The American Society of Gene & Cell Therapy

A Phase I Study of Telomerase-specific Replication Competent Oncolytic Adenovirus (Telomelysin) for Various Solid Tumors

John Nemunaitis[1–4], Alex W Tong[3,4], Michael Nemunaitis[1], Neil Senzer[1–4], Anagha P Phadke[4], Cynthia Bedell[1], Ned Adams[1], Yu-An Zhang[3,4], Phillip B Maples[4], Salina Chen[4], Beena Pappen[4], James Burke[5], Daiju Ichimaru[6], Yasuo Urata[6] and Toshiyoshi Fujiwara[7]

[1]Mary Crowley Cancer Research Centers, Dallas, Texas, USA; [2]Texas Oncology PA, Dallas, Texas, USA; [3]Baylor Sammons Cancer Center, Dallas, Texas, USA; [4]Gradalis, Inc., Dallas, Texas, USA; [5]Billings Clinic, Billings, Montana, USA; [6]Oncolys BioPharma, Tokyo, Japan; [7]Center for Gene and Cell Therapy, Okayama University Hospital, Okayama, Japan

A phase I clinical trial was conducted to determine the clinical safety of Telomelysin, a human telomerase reverse transcriptase (hTERT) promoter driven modified oncolytic adenovirus, in patients with advanced solid tumors. A single intratumoral injection (IT) of Telomelysin was administered to three cohorts of patients (1×10^{10}, 1×10^{11}, 1×10^{12} viral particles). Safety, response and pharmacodynamics were evaluated. Sixteen patients with a variety of solid tumors were enrolled. IT of Telomelysin was well tolerated at all dose levels. Common grade 1 and 2 toxicities included injection site reactions (pain, induration) and systemic reactions (fever, chills). hTERT expression was demonstrated at biopsy in 9 of 12 patients. Viral DNA was transiently detected in plasma in 13 of 16 patients. Viral DNA was detectable in four patients in plasma or sputum at day 7 and 14 post-treatment despite below detectable levels at 24 h, suggesting viral replication. One patient had a partial response of the injected malignant lesion. Seven patients fulfilled Response Evaluation Criteria in Solid Tumors (RECIST) definition for stable disease at day 56 after treatment. Telomelysin was well tolerated. Evidence of antitumor activity was suggested.

Received 16 July 2009; accepted 15 October 2009; advance online publication 24 November 2009. doi:10.1038/mt.2009.262

INTRODUCTION

Conditionally replicative oncolytic viruses are engineered to replicate selectively in cancer cells with specified oncogenic phenotypes. Multiple viral backbones have been employed, although the most commonly utilized is derived from the adenovirus serotype 5.

Two different approaches have been used to limit adenoviral replication to cancer cells. One approach is to delete components of viral genes (*E1A*, *E1B*) that function in part to neutralize normal cell defense (p53, Rb) mechanisms. Loss of function of the cell defense genes in cancer cells renders the virus cytotoxic to tumor cells but incapable of replication in normal cells, as exemplified by ONYX-015 or Δ24.[1] Alternatively, native viral promoters that govern the initiation of viral replication can be replaced with a promoter region for genes that are active and/or overexpressed in cancer cells.[2,3] The resulting constructs display viral cytolytic activity that is confined to cancer cells but at a level that approaches that of wild-type adenovirus.[2] Numerous studies have confirmed that administration of live, wild-type adenovirus to healthy, adult humans is safe.[3]

Telomelysin is a novel, replication-competent adenovirus serotype 5-based adenoviral construct that incorporates a human telomerase reverse transcriptase gene (*hTERT*) promoter. *hTERT* encodes for the catalytic protein subunit of telomerase, a polymerase that acts to stabilize telomere lengths and is highly expressed in tumors but not in normal, differentiated adult cells.[4,5]

Additional modifications of Telomelysin include the replacement of the normal transcriptional element of viral *E1B* gene by an IRES (Internal Ribosomal Entry Site) sequence to minimize "leakiness" further enhancing specificity. Furthermore, Telomelysin is the first replication-competent adenovirus that retains a fully functional viral E3 region.[6]

In vitro studies have validated the selective infectivity and direct cytolysis of Telomelysin in cancer cells but not nonmalignant cells.[5] In animal experiments, intratumoral injection (IT) of Telomelysin demonstrated antitumor activity without significant toxicity to normal organs. Additionally, distant viral uptake was observed following IT evidenced by the presence of adenoviral protein identified in noninjected tumor following intratumoral treatment of the contralateral tumor.[5]

These encouraging preclinical findings of safety and directed antitumor activity form the basis of our phase I study, which is designed to validate safety, response and pharmacodynamics of Telomelysin in advanced cancer patients.

RESULTS

Patient profile

Sixteen patients were entered into trial: three each into cohorts 1 and 2 and 10 into cohort 3. The age, sex, histological diagnosis, and prior treatments of the evaluated patients are shown in **Table 1**.

Correspondence: *John Nemunaitis, 1700 Pacific Avenue, Suite 1100, Dallas, Texas 75201, USA. E-mail: jnemunaitis@marycrowley.org*

© The American Society of Gene & Cell Therapy

Table 1 Patient demographics

Patient	Age	Sex	Histological diagnosis	Prior treatments
1 (101)	57	F	Squamous cell ca unknown primary	XRT, carboplatin, docetaxel, anastrozole
2 (102)	54	M	Melanoma	Interferon, dacarbazine
3 (103)	34	F	Melanoma	Lenalidomide, dacarbazine, vinblastine, cisplatin, IL-2, interferon
4 (204)	60	M	Salivary gland tumor	XRT, perifosine
5 (205)	69	M	Squamous cell ca base of tongue	Cisplatin, XRT
6 (206)	60	F	Leiomyosarcoma	Doxorubicin, ifosfamide, gemcitabine, docetaxel, perifosine
7 (307)	52	F	Neuroendocrine tumor	Irinotecan, cisplatin, topotecan, docetaxel, pemetrexed, CT 2103, XRT
8 (308)	78	F	Melanoma	Interferon
9 (309)	54	M	NSCLC	Paclitaxel, carboplatin, pemetrexed, XRT
10 (310)	49	M	Squamous cell ca base of tongue	Paclitaxel, carboplatin, cisplatin, fluorouracil, cetuximab, XRT
11 (311)	60	M	Squamous cell ca floor of mouth	Cisplatin, XRT
12 (312)	48	M	Melanoma	Interferon, melphalan, actinomycin-D
13 (313)	54	F	Sarcoma	None
14 (314)	38	M	Basal cell carcinoma	Cisplatin, fluorouracil
15 (315)	54	F	Squamous cell ca of gall bladder	Capecitabine, gemcitabine
16 (316)	46	F	Breast cancer	Doxorubicin, cyclophosphamide, paclitaxol, herceptin, tamoxifen, anastrozole, capecitabine, docetaxel

M, male; F, Female.

Adverse events

No clinically significant grade 3 or 4 treatment related toxic events were experienced by any patients. There were multiple grade 1 and 2 adverse events, with the most common being fever, chills, fatigue, and injection site pain (Table 2). Thirteen patients developed asymptomatic transient lymphocyte decreases, seven grade 2, five grade 3 and one grade 4, 24 hours after Telomelysin injection with complete recovery by day 7 following injection.

Clinical response

Eleven patients satisfied Response Evaluation Criteria in Solid Tumors (RECIST) criteria for stable disease response to the injected lesion at Day 28, three had progressive disease and two more unevaluable. Seven of the day 28 stable disease patients had stable disease at day 56, two had progressive disease and two were unevaluable. One patient (pt 308) had 33% reduction of injected lesion at day 28 and 56.7% reduction of injected lesion at day 56 (see Figure 1).

Table 2 List of common[a] adverse events

	Grade 1	Grade 2	Grade 3, 4	Overall ($N = 16$)
Cardiac arrhythmia				
Supraventricular and nodal arrhythmia—sinus tachycardia	2	1	0	3
Gastrointestinal				
Nausea	3	1	0	4
Constitutional Sypmtoms				
Chills	1	5	0	6
Fatigue	7	2	0	9
Edema peripheral	1	2	0	3
Fever	3	3	0	6
Pain				
Bone	2	1	0	3
Muscle	0	3	0	3
Extremity	2	1	0	3
Pain	3	1	0	4
Headache	3	1	0	4
Pulmonary/upper respiratory				
Nasal cavity/paranasal reactions	2	1	0	3
Dermatology/skin				
Erythema	0	0	3	3
Injection site bruising	3	0	0	3
Injection site erythema	1	4	0	5
Injection site pain	4	2	0	6

[a]Occurring in >15% of patients ($n = 16$).

Postinjection biopsies performed at day 28 on four of the patients with stable disease revealed necrosis that may or may not be treatment induced. Three of these patients had melanoma. Survival of all patients ranged from 1 to 21 months (median 10).

Viral pharmacokinetics analysis

Systemic dissemination of Telomelysin was evaluated by collection of patient plasma, urine, sputum, and saliva at time points before and after IT. Quantitative real-time PCR analysis was carried out with primers that were specific for the Telomelysin E1A and IRES regions. We detected the presence of viral DNA in 13 of 16 patient plasma samples tested, including 9 of 10 patients in cohort 3 (Table 3). Plasma viral DNA was detected between 30 minutes and 6 hours in most patients, at concentrations that ranged from 2.1×10^3 to 1.5×10^7 viral copies/ml. We detected the presence of plasma viral particles in two cohort 3 patients. Viral DNA copies detected on day 7 (pt 312: 3.7×10^3; pt 316: 2×10^4 viral copies/ml, respectively) were ~10–50-fold higher than detection threshold (400 vp/ml). Viral DNA was also detected in one cohort 2 patient on days 7 and 14 [pt 205: 3.7×10^3 (day 7), 6.0×10^3 (day 14)] but not at (Figure 2). No viral DNA was detected at 24 hours post-treatment for these patients, suggesting that detectable levels of viral DNA at days 7 and 14 may constitute a second

© The American Society of Gene & Cell Therapy

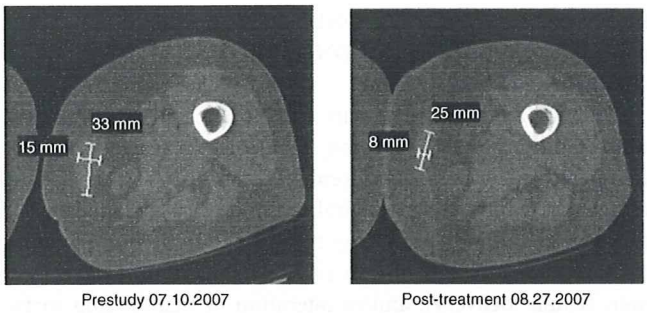

Figure 1 Patient 308: Initial response of the largest of three metastatic melanoma lesions involving the right thigh.

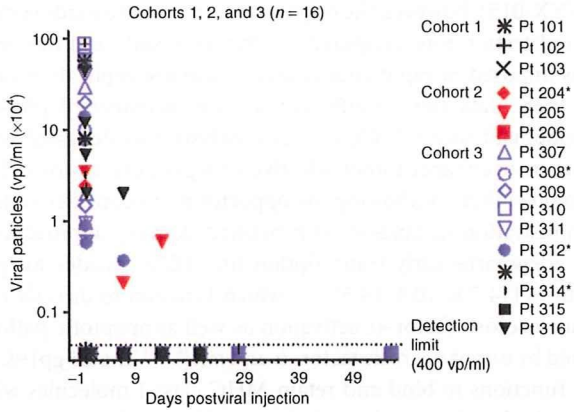

Figure 2 Detection of Telomelysin viral DNA in patient plasma samples on various days post-treatment. Data represented at day 1 constituted peak values determined at up to 6 hours post-treatment. All patients exhibited below detection levels of plasma viral particles (≤400 vp/ml) at day 1 post-treatment.

wave of viremia from replication. Viral DNA was detected in two cohort 3 sputum specimens on day 1 (pt 310: 8.2×10^4 viral copies/ml) and day 7 (pt 307, 5×10^3 viral copies/ml) but not at earlier time points post-treatment. Viral DNA was not detected in any other body fluid compartments examined. The systemic detection of viral DNA at these extended time points is suggestive of viral replicative activity.

Viral E1A and hexon expression in treated tumors

Immunohistochemical evaluation of adenoviral hexon protein expression in treated tumor biopsies was carried out as a surrogate indicator of viral replicative activity at days 28 and 56 postinjection. Viral hexon protein expression was not detected in Telomelysin treated tumor biopsies collected at days 28 and 56 from 15 of 16 patients (Table 3), whereas one patient displayed an equivocal reaction at day 56 but not day 28. Viral E1A expression was uniformly negative from all 16 patients. The negative findings indicate that viral replicative activity did not extend to these time points, despite suggestion of viral dissemination for up to day 7–14 after the single viral injection.

Neutralizing antibody response

To identify systemic immune-activating events from intratumoral Telomelysin treatment, a functional assay with Telomelysin-infected HEK 293 cells was used to determine the neutralizing antibody (NAb) titer of patients entered into trial. Blocking activity of graded concentrations of the patient's pre- and post-treatment plasma was determined by light microscopy. An elevated NAb titer was observed in 14 of 14 plasma samples collected at day 28 (Table 3). Two patients (pt 313 and pt 316) did not have samples collected. The increase in titer ranged from 8- to 512-fold (Figure 3). However, the magnitude of titer increase did not correlate either with dose or with the presence or absence of a pre-existing NAb titer (Figure 3).

Table 3 Pharmacokinetics and immune response assessments

	No. positive[a]/No. tested			
Analyses performed[a]	Total	Cohort 1	Cohort 2	Cohort 3
Viral DNA in plasma	13/16	2/3	2/3	9/10
Viral DNA in sputum	2/16	0/3	0/3	2/10
Viral DNA in urine and saliva	0/16	0/3	0/3	0/10
Endogenous hTERT expression	9/12[b]	2/3	1/1	6/8
ADV neutralizing antibody (D28)	14/14	3/3	3/3	8/8[c]
Viral plaque assay	3/16	0/3	0/3	3/10
Serum IL-6	8/9[d]	3/3	2/3	3/3
Serum IL-10	7/9[d]	2/3	2/3	3/3
Serum IFN-γ	2/9[d]	2/3	0/3	0/3
In situ viral hexon (D56)	1/16	0/3	0/3	1/10
Lymphocyte subset alterations by immunophenotyping analysis	0/10	0/0	0/0	0/10

[a]Positive at any post-treatment time point tested. [b]12 of 15 patients with adequately recovered RNA were analyzed. [c]d28 plasma samples were not collected from patients 313 and 316 in cohort 3. [d]Only first 3 patients per cohort were analyzed, per protocol.

Serum cytokines

Non specific systemic immune activation from intratumoral Telomelysin treatment was observed as evidenced by an elevated increase in serum cytokine levels, in particular, interleukin-6 (IL-6) and IL-10 in all cohorts (Table 3). An elevated IL-6 level (>50%) was observed in 8 of 9 patients tested, as early as 30 minutes after treatment. Increased IL-10 level was also observed in 7 of 9 patients, whereas two patients had elevated interferon-γ.

Peripheral blood lymphocyte immunophenotyping

There were no demonstrable trends of altered post-treatment changes in the frequency distribution of $CD4^+$ T, $CD8^+$ T, B, and NK cells that correlated with viral treatment (Table 3) in 10 tested patients.

hTERT mRNA

To validate viral replication permissiveness of injected tumor specimens, real time, quantitative real-time-PCR assays were carried out retrospectively using tumor biopsy specimens collected before treatment, using total RNA from frozen patient tumor biopsy and primers and a TaqMan probe specific to hTERT or the

© The American Society of Gene & Cell Therapy •

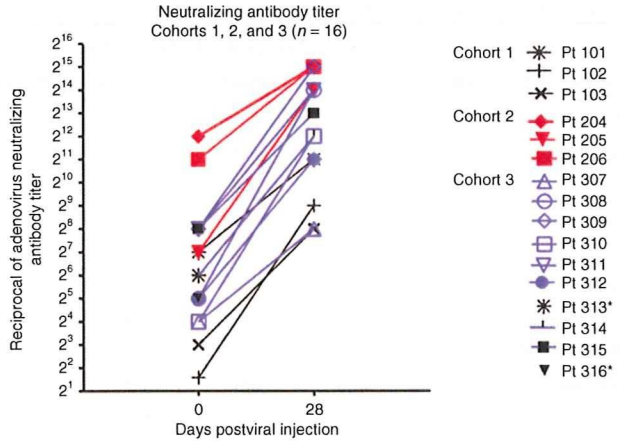

Figure 3 Neutralizing antibody titer. Change in neutralizing antibody titer on day 28 after injection compared to baseline. *Patients 313 and 316 did not have day 28 plasma samples to determine post-treatment neutralizing antibody titer.

housekeeping gene *GAPDH* (glyceraldehyde-3-phosphate dehydrogenase). Tumor hTERT expression was carried out in 12 of 15 tumor biopsies that yielded adequate RNA. Tumor biopsy was not available from pt 316. Endogenous hTERT expression was detected in 9 of the 12 tumor biopsy specimens (Table 3). These included two with high hTERT (>10^4 copies/μg) mRNA expression (one in cohort 2 and one in cohort 3), four with moderate expression (10^3–10^4 copies/μg) (one in cohort 1, three in cohort 3), and three with low expression (≤10^3 copies/μg) (one in cohort 1, two in cohort 3). hTERT was below detection limit in three other patients tested (one in cohort 1, two in cohort 3). Of the three patients with prolonged, detectable plasma viral DNA at day 7 post-treatment, pt 205 displayed a high level of endogenous hTERT mRNA, whereas tumor samples were either unavailable (pt 316) or inadequate (pt 312) for assessment. These limited findings confirm hTERT expression in the majority of human tumors.

DISCUSSION

Telomelysin administration in this Phase I safety trial demonstrated safety with no treatment related grade 3/4 adverse effects. Further, we observed the encouraging findings of one patient with partial response at day 56 after a single IT. The transient presence of systemic Telomelysin dissemination following IT was documented early after IT injection. Immune activation was observed, with cytokine upregulation of IL-6 and IL-10 and the induction of viral neutralizing antibodies. Limited suggestive evidence of vial replication was observed at day 7 post-treatment in three patients, for whom plasma viremia was not detected on day 1. One of these three patients had elevated malignant tissue hTERT expression with a significant clinical response. However, these limited findings require additional confirmation as we cannot completely exclude the unlikely possibility of delayed viral clearance. Immunohistochemical analysis of viral E1A and hexon was negative 28 days after injection suggesting rapid clearance. In Galanis' Phase II osteosarcoma trial with ONYX-015, 5 of 6 patients had detectable viral DNA on Day 5 of the first cycle.[7] In Makower's hepatobiliary tumor trial with ONYX-015, no viral DNA was detected in plasma following intralesional injection.[8] In our previous work with ONYX-015 we showed that 41% of patients had detectable viral DNA at days 5 and 6, and 9% had circulating DNA at day 10.

Adenoviral immunogenicity can be affected by viral structural modification (E3 region function), physical properties (temperature), other agents (enbrel, steroids), serotype status, removal of neutralizing antiviral antibodies (plasmapheresis) or presence of antibody producing cells (B-cell inhibition secondary to Ribavirin, Rituxan), use of physical shields (liposome, polymer, cellular delivery), and/or alteration of neutralizing surface epitopes (hexon, knob, fiber).[9–32]

Evidence of clinical efficacy has previously been demonstrated with a *E1B-55* kd deleted oncolytic adenoviral therapeutic (ONYX-015); however, the opportunity to move towards systemic administration was hampered by efficacy results and the limitations imposed by rapid viral clearance and low replication capacity. These data were insufficient for advancement of phase III development with ONYX-015. Telomelysin was designed with a structure to enhance tumor selective viral gene expression (*hTERT* promoter) thereby allowing the opportunity to consider systemic administration in tandem with masked delivery approaches.[33,34] The adenovirus early transcription unit (E3) encodes for polypeptides (14.7 k, 10.4, 14.5),[35–39] which function to directly block tumor necrosis factor–α activation as well as apoptotic pathways shared by tumor necrosis factor–α and *fas*.[38,40,41] The E3 gp19k protein functions to bind and retain MHC class I molecules within the endoplasmic reticulum, thus preventing surface presentation of viral antigens, thereby limiting class I-restricted CTL clearance of virally infected cells.[35,36,42–45] The expression of the E3 gene region products may, therefore, decrease viral clearance, increase the expression of those viral genes that suppress immune recognition and enhance viral replication.[40,46]

In conclusion, both activity and safety of a single injection approach for Telomelysin has been demonstrated. However, despite activity in a subset of patients, limited clinical relevant responses were observed in others. This may be attributed to the single viral treatment administered to each patient. An increase in viral NAb titer in all patients tested is indicative of systemic immune sensitization following IT. We and others have shown previously that systemic viremia can be maintained at 3–6 days after second intravenous or intra-arterial treatments in spite of the presence of high levels of NAb titers and antiviral cytokines.[47,48] Thus repeat intratumoral or intranvenous injection of Telomelysin is a viable treatment option to achieve an improved clinical response. Alternatively, artificial envelopment of Telomelysin with bilamellar cationic liposomes for "stealth" systemic delivery may be applicable for improving systemic pharmacokinetics and coxsackie and adenovirus receptor-independent tropism.[33,34] With these considerations, data support further clinical assessment of a multi treatment schedule.

MATERIALS AND METHODS

Test article. Telomelysin is manufactured at Introgen Therapeutics, Houston, TX. Telomelysin was reconstituted using aseptic technique in a Biocontainment Level 2 ISO Class 5 Biosafety Cabinet.

Study design. This was a dose escalation study in patients with advanced solid tumors. A single IT of virus particles (vp) was administered through a single injection site using a radial method of distribution in order to evenly

© The American Society of Gene & Cell Therapy

distribute material to both peripheral and central sites of growing tumor without removing the needle completely from the tumor. Most of the viral dose was administered at the tumor periphery and at the interface between normal tissue and tumor; prior studies have indicated improved efficacy with this administration approach.[49] Attempts were made to distribute the virus uniformly along the needle tracks by gradually depressing the syringe plunger during withdrawal of the needle. Each patient was enrolled into one of the following cohorts: Cohort 1: 1×10^{10} vp/tumor ($n = 3$); Cohort 2: 1×10^{11} vp/tumor ($n = 3$); Cohort 3: 1×10^{12} vp/tumor ($n = 10$). Patients in cohorts 1 and 2 remained on study for 28 days after injection. Cohort 3 patients were followed until day 56 post-treatment.

Viral DNA was monitored using quantitative PCR (Q-PCR) technique. After the first patient was enrolled into Cohort 1, each of the remaining patients (*i.e.*, pt 2 and pt 3) was enrolled. In Cohort 1, clearance of viral DNA in all body fluid specimens including blood, saliva, sputum, and urine of the preceding patients by two consecutive negative Q-PCR results at least 3 days apart was required. Enrollment of the first patient in Cohort 2 began when viral DNA results on the last patient in Cohort 1 were negative on two consecutive tests at least 3 days apart.

If a dose-limiting toxicity was observed in one of three patients related to Telomelysin, an additional three patients were enrolled. If only one of the six total patients experienced a dose-limiting toxicity, then the dose escalation would be continued to the next cohort. If two or more of the six patients experienced a dose-limiting toxicity, the maximum tolerated dose would be defined as exceeded and an additional three patients would be treated at the dose level below. Toxicities were graded and reported according to the National Cancer Institute common terminology criteria for adverse events, version 3.0. Response was evaluated in this study using the international criteria proposed by the RECIST Committee.

Study population. Patients with superficial accessible cancer who had failed at least one prior therapeutic regimen and for whom effective conventional therapy was not available were eligible for the study. All patients were required to be at least 18 years old, have histologically confirmed carcinoma and a Karnofsky performance status of at least 70%. Inclusion was also predicated on normal laboratory assessment. All patients were required to provide written consent according to local institutional review board–approved guidelines. Women and men of reproductive potential were required to use contraception.

Baseline assessments included: concomitant medications, interval history, physical examination, performance status, tumor assessment, medical laboratory studies, adenoviral NAb, urinalysis, tumor biopsy, viral DNA in blood, saliva, sputum, and urine. Viral plaque forming titer in serum, cytokine levels (IL-6, IL-10, INF-γ). Peripheral blood immunephenotype analyses were performed for Cohort 3 patients.

Assessments were performed using samples collected as follows: plasma viral DNA: pretreatment and at 30 minutes, 1 hour, 3 hours, 6 hours and on days 1, 7, 14, 21, 28, and 56 post-treatment; viral DNA in sputum, urine, and saliva: pretreatment and days 1, 7, 14, 21, 28, and 56 postinjection; endogenous hTERT expression: assessed with pretreatment tumor biopsy; adenovirus NAb: pretreatment and day 28 post-treatment; cytokine: pretreatment and 30 minutes, 1 hour, 6 hours, and on days 1, 14, and 28 post-treatment for first three patients per cohort only; immunohistochemistry for viral hexon: tumor biopsies collected pretreatment and on days 28 and day 56 post-treatment; immunephenotyping analysis: pretreatment and days 7, 14, and 28 post-treatment. Viral plaque assay was performed only on patient plasma samples that yielded $\geq 1 \times 10^5$ vp/ml by Q-PCR analysis.

Detection of viral DNA. Patient samples were collected previral infusion and on day 0 (1 hour, 3 hours, 6 hours post-treatment), day 1, 7, 14, 21, 28, and 56 post-IT. DNA extraction was carried out from patient's archived, frozen tumor biopsy specimen, plasma, sputum, saliva, and urine specimens. Viral DNA was quantified by real-time Q-PCRs. Briefly, DNA was extracted with the Qiagen QIAmp DNA Mini Kit (plasma and saliva samples) or QIAamp Viral RNA Mini Kit (urine and sputum samples). Plasma, saliva, sputum, and urine samples from normal donors were used for protocol validation, with or without "spiking" with known amounts of Telomelysin immediately prior to DNA extraction. Q-PCRs were carried out on the iQ5 Q-thermal cycler (BioRad, Hercules, CA), using Telomelysin-specific primers for the E1A and IRES region and the 2 × Power SYBR Green PCR Master Mix (Applied Biosystems, Foster City, CA). The amounts of detectable viral particles were quantified by extrapolation with a standard curve, generated with serially diluted (1:10) DNA templates with predetermined copy numbers (10 to 1×10^6 copies) of pure Telomelysin viral DNA. A positive response is based on the detection of both IRES- and E1A amplification products with an assay threshold of 4×10^2 vp/ml for plasma and saliva; 1×10^3 vp/ml for urine; 2×10^3 vp/ml for sputum samples for both reactions.

Primer sequences

IRES-Forward 5′-GAT TTT CCA CCA TAT TGC CG
IRES-Reverse 5′-TTC ACG ACA TTC AAC AGA CC
E1A-Forward 5′-CCT GTG TCT AGA GAA TGC AA
E1A-Reverse 5′-ACA GCT CAA GTC CAA AGG TT.

Endogenous hTERT expression in patient tumor. To validate viral replication, real time, quantitative real-time-PCR assays were carried out with total RNA from patient tumor biopsy. Briefly, Q-PCR assays were carried out on iQ5 Q-PCR machine (BioRad), using primers and a TaqMan probe specific to hTERT or GAPDH (Sigma/Proligo, St Louis, MO), and TaqMan Core PCR reagents (Applied Biosystems). Total RNA was extracted with the RNeasy Mini Kit (Qiagen, Valencia, CA). cDNAs were generated according to manufacturer's instructions (RETROscript kit; Ambion, Foster City, CA). PCR standard curves for determination of gene copy number in the reaction template were generated with triplicate reactions, using 1:10, serially diluted samples of either the hTERT or GAPDH PCR amplification products.

Primer sequences

hTERT Forward primer: 5′-GCACTGGCTGATGAGTGTGT-3′
hTERT Reverse primer: 5′- CTCGGCCCTCTTTTCTCTG-3′
hTERT TaqMan probe: 5′-(FAM) TTGCAAAGCATTGGAATCAGA CAGCACT-(TAMRA)-3′
GAPDH Forward primer: 5′-GAAGGTGAAGGTCGTAGTC-3′
GAPDH Reverse primer: 5′-GAAGATGGTGATGGGATTTC-3′
GAPDH TaqMan probe: 5′-(FAM) CAAGCTTCCCGTTCTCAGCC (TAMRA)-3′.

Immunohistochemical analysis. A previously described automated immunoperoxidase staining technique was used to characterize viral protein expression.[50] Briefly, viral E1A and hexon expression was determined with the avidin-biotin-complexed immunoperoxidase reaction (*i*VIEW DAB Detection kit; Ventana Medical Systems, Tucson, AZ) following initial incubation with antibodies specific to viral E1A (prediluted mouse monoclonal adenovirus type 5 E1A antibody, GeneTex, Irvine, CA), or hexon (goat antiadenovirus polyclonal antibody (Millipore, Billerica, MA), using the Ventana 320ES System (Ventana Medical Systems, Tucson, AZ).

Flow cytometric immunophenotype analysis. Peripheral blood immunophenotype analysis was carried by a two color immunofluorescence reaction and flow cytometric analysis as described previously.[50] The frequency distribution of T, B, and NK cell subsets: CD45-FITC/CD14-PE, CD3-FITC/CD19-PE, CD4-FITC/CD8-PE, CD13-FITC [CD16 CD56]-PE (all from BD Biosciences, San Jose, CA) were determined.

Serum cytokine analysis. ELISA assays (R&D Quantikine kits, Minneapolis, MN) were used to quantify patient serum cytokine levels.[50] Serial serum samples were analyzed simultaneously, using cytokine-specific immunoassay reagents. The colorimetric reaction was quantified as a function of optical density absorbance at 450 nm with the correction wavelength set at 540 nm

© The American Society of Gene & Cell Therapy

(SpectraMax 340; Molecular Devices, Sunnyvale, CA). The minimal detectable concentration was as follows: interferon-γ: <16 pg/ml; IL-10: <8 pg/ml; IL-6: <1 pg/ml. The percent increase in cytokine level at any time point post-treatment was determined through comparison with serum harvested before Telomelysin injection. Based on inter- and intra-sample variations, increases in cytokine level of ≥50% over baseline were considered significant.

Antiadenovirus antibodies. Adenovirus-NAb titer in patient plasma samples was measured as a function of blocking human adenovirus infection of 293 cells. Briefly, twofold serially diluted patient plasma samples were added to 293 cells that were infected with Telomelysin virus. The plates were evaluated microscopically for the percentage of cells that lysed in presence of patient plasma samples at 72 and 96 hours postinfection. The adenovirus-NAb titer for a given sample was the highest dilution of the plasma that showed a blocking effect (>60% 293 cells intact and attached as monolayer).

ACKNOWLEDGMENTS

We acknowledge Susan Mill and Brenda Marr for their competent and knowledgeable assistance in the preparation of this manuscript.

REFERENCES

1. Tong AW (2006). Oncolytic Viral Therapy for Human Cancer: Challenges Revisited (review). *Drug Development Research* **66**: 260–277.
2. Taki, M, Kagawa, S, Nishizaki, M, Mizuguchi, H, Hayakawa, T, Kyo, S *et al.* (2005). Enhanced oncolysis by a tropism-modified telomerase-specific replication-selective adenoviral agent OBP-405 ('Telomelysin-RGD'). *Oncogene* **24**: 3130–3140.
3. Lichtenstein, DL and Wold, WS (2004). Experimental infections of humans with wild-type adenoviruses and with replication-competent adenovirus vectors: replication, safety, and transmission. *Cancer Gene Ther* **11**: 819–829.
4. Shay, JW, Zou, Y, Hiyama, E and Wright, WE (2001). Telomerase and cancer. *Hum Mol Genet* **10**: 677–685.
5. Kawashima, T, Kagawa, S, Kobayashi, N, Shirakiya, Y, Umeoka, T, Teraishi, F *et al.* (2004). Telomerase-specific replication-selective virotherapy for human cancer. *Clin Cancer Res* **10**(1 Pt 1): 285–292.
6. Lichtenstein, DL, Toth, K, Doronin, K, Tollefson, AE and Wold, WS (2004). Functions and mechanisms of action of the adenovirus E3 proteins. *Int Rev Immunol* **23**: 75–111.
7. Galanis, E, Okuno, SH, Nascimento, AG, Lewis, BD, Lee, RA, Oliveira, AM *et al.* (2005). Phase I-II trial of ONYX-015 in combination with MAP chemotherapy in patients with advanced sarcomas. *Gene Ther* **12**: 437–445.
8. Makower, D, Rozenblit, A, Kaufman, H, Edelman, M, Lane, ME, Zwiebel, J *et al.* (2003). Phase II clinical trial of intralesional administration of the oncolytic adenovirus ONYX-015 in patients with hepatobiliary tumors with correlative p53 studies. *Clin Cancer Res* **9**: 693–702.
9. Pan, Q, Liu, B, Liu, J, Cai, R, Wang, Y and Qian, C (2007). Synergistic induction of tumor cell death by combining cisplatin with an oncolytic adenovirus carrying TRAIL. *Mol Cell Biochem* **304**: 315–323.
10. Nemunaitis, J, Senzer, N, Sarmiento, S, Zhang, YA, Arzaga, R, Sands, B *et al.* (2007). A phase I trial of intravenous infusion of ONYX-015 and enbrel in solid tumor patients. *Cancer Gene Ther* **14**: 885–893.
11. Lin, E and Nemunaitis, J (2004). Oncolytic viral therapies. *Cancer Gene Ther* **11**: 643–664.
12. Wolff, G, Worgall, S, van Rooijen, N, Song, WR, Harvey, BG and Crystal, RG (1997). Enhancement of *in vivo* adenovirus-mediated gene transfer and expression by prior depletion of tissue macrophages in the target organ. *J Virol* **71**: 624–629.
13. Fisher, KD, Green, NK, Hale, A, Subr, V, Ulbrich, K and Seymour, LW (2007). Passive tumour targeting of polymer-coated adenovirus for cancer gene therapy. *J Drug Target* **15**: 546–551.
14. Fujiwara, T, Urata, Y and Tanaka, N (2007). Telomerase-specific oncolytic virotherapy for human cancer with the hTERT promoter. *Curr Cancer Drug Targets* **7**: 191–201.
15. Fujiwara, T, Urata, Y and Tanaka, N (2008). Diagnostic and therapeutic application of telomerase-specific oncolytic adenoviral agents. *Front Biosci* **13**: 1881–1886.
16. Doronin, K, Toth, K, Kuppuswamy, M, Krajcsi, P, Tollefson, AE and Wold, WS (2003). Overexpression of the ADP (E3-11.6K) protein increases cell lysis and spread of adenovirus. *Virology* **305**: 378–387.
17. Delgado-Enciso, I, Cervantes-García, D, Martínez-Dávila, IA, Ortiz-López, R, Alemany-Bonastre, R, Silva-Platas, CI *et al.* (2007). A potent replicative delta-24 adenoviral vector driven by the promoter of human papillomavirus 16 that is highly selective for associated neoplasms. *J Gene Med* **9**: 852–861.
18. Kim, E, Kim, JH, Shin, HY, Lee, H, Yang, JM, Kim, J *et al.* (2003). Ad-mTERT-delta19, a conditional replication-competent adenovirus driven by the human telomerase promoter, selectively replicates in and elicits cytopathic effect in a cancer cell-specific manner. *Hum Gene Ther* **14**: 1415–1428.
19. Vile, RG and Hart, IR (1993). *In vitro* and *in vivo* targeting of gene expression to melanoma cells. *Cancer Res* **53**: 962–967.
20. Savontaus, MJ, Sauter, BV, Huang, TG and Woo, SL (2002). Transcriptional targeting of conditionally replicating adenovirus to dividing endothelial cells. *Gene Ther* **9**: 972–979.
21. Shirakawa, T, Hamada, K, Zhang, Z, Okada, H, Tagawa, M, Kamidono, S *et al.* (2004). A cox-2 promoter-based replication-selective adenoviral vector to target the cox-2-expressing human bladder cancer cells. *Clin Cancer Res* **10**: 4342–4348.
22. Douglas, JT, Rogers, BE, Rosenfeld, ME, Michael, SI, Feng, M and Curiel, DT (1996). Targeted gene delivery by tropism-modified adenoviral vectors. *Nat Biotechnol* **14**: 1574–1578.
23. Haisma, HJ, Pinedo, HM, Rijswijk, A, der Meulen-Muileman, I, Sosnowski, BA, Ying, W *et al.* (1999). Tumor-specific gene transfer via an adenoviral vector targeted to the pan-carcinoma antigen EpCAM. *Gene Ther* **6**: 1469–1474.
24. Goldman, CK, Rogers, BE, Douglas, JT, Sosnowski, BA, Ying, W, Siegal, GP *et al.* (1997). Targeted gene delivery to Kaposi's sarcoma cells via the fibroblast growth factor receptor. *Cancer Res* **57**: 1447–1451.
25. Miller, CR, Buchsbaum, DJ, Reynolds, PN, Douglas, JT, Gillespie, GY, Mayo, MS *et al.* (1998). Differential susceptibility of primary and established human glioma cells to adenovirus infection: targeting via the epidermal growth factor receptor achieves fiber receptor-independent gene transfer. *Cancer Res* **58**: 5738–5748.
26. Grill, J, Van Beusechem, VW, Van Der Valk, P, Dirven, CM, Leonhart, A, Pherai, DS *et al.* (2001). Combined targeting of adenoviruses to integrins and epidermal growth factor receptors increases gene transfer into primary glioma cells and spheroids. *Clin Cancer Res* **7**: 641–650.
27. Ulasov, IV, Zhu, ZB, Tyler, MA, Han, Y, Rivera, AA, Khramtsov, A *et al.* (2007). Survivin-driven and fiber-modified oncolytic adenovirus exhibits potent antitumor activity in established intracranial glioma. *Hum Gene Ther* **18**: 589–602.
28. Zhang, YA, Nemunaitis, J, Samuel, SK, Chen, P, Shen, Y and Tong, AW (2006). Antitumor activity of an oncolytic adenovirus-delivered oncogene small interfering RNA. *Cancer Res* **66**: 9736–9743.
29. Alonso, MM, Gomez-Manzano, C, Bekele, BN, Yung, WK and Fueyo, J (2007). Adenovirus-based strategies overcome temozolomide resistance by silencing the O6-methylguanine-DNA methyltransferase promoter. *Cancer Res* **67**: 11499–11504.
30. Lamfers, ML, Idema, S, Bosscher, L, Heukelom, S, Moeniralm, S, van der Meulen-Muileman, IH *et al.* (2007). Differential effects of combined Ad5- delta 24RGD and radiation therapy in *in vitro* versus *in vivo* models of malignant glioma. *Clin Cancer Res* **13**: 7451–7458.
31. DeWeese, TL, van der Poel, H, Li, S, Mikhak, B, Drew, R, Goemann, M *et al.* (2001). A phase I trial of CV706, a replication-competent, PSA selective oncolytic adenovirus, for the treatment of locally recurrent prostate cancer following radiation therapy. *Cancer Res* **61**: 7464–7472.
32. Kawakami, K, Takeshita, F and Puri, RK (2001). Identification of distinct roles for a dileucine and a tyrosine internalization motif in the interleukin (IL)-13 binding component IL-13 receptor alpha 2 chain. *J Biol Chem* **276**: 25114–25120.
33. Yotnda, P, Chen, DH, Chiu, W, Piedra, PA, Davis, A, Templeton, NS *et al.* (2002). Bilamellar cationic liposomes protect adenovectors from preexisting humoral immune responses. *Mol Ther* **5**: 233–241.
34. Thompson, DH (2008). Adenovirus in a synthetic membrane wrapper: an example of hybrid vigor? *ACS Nano* **2**: 821–826.
35. Ilan, Y, Droguett, G, Chowdhury, NR, Li, Y, Sengupta, K, Thummala, NR *et al.* (1997). Insertion of the adenoviral E3 region into a recombinant viral vector prevents antiviral humoral and cellular immune responses and permits long-term gene expression. *Proc Natl Acad Sci USA* **94**: 2587–2592.
36. Lee, MG, Abina, MA, Haddada, H and Perricaudet, M (1995). The constitutive expression of the immunomodulatory gp19k protein in E1-, E3- adenoviral vectors strongly reduces the host cytotoxic T cell response against the vector. *Gene Ther* **2**: 256–262.
37. Wold, WS, Hermiston, TW and Tollefson, AE (1994). Adenovirus proteins that subvert host defenses. *Trends Microbiol* **2**: 437–443.
38. Wold, WS, Tollefson, AE and Hermiston, TW (1995). E3 transcription unit of adenovirus. *Curr Top Microbiol Immunol* **199** (Pt 1): 237–274.
39. Bett, AJ, Haddara, W, Prevec, L and Graham, FL (1994). An efficient and flexible system for construction of adenovirus vectors with insertions or deletions in early regions 1 and 3. *Proc Natl Acad Sci USA* **91**: 8802–8806.
40. Wittmann, W, Fabricius, EM, Schneeweiss, U, Schaepe, C, Benedix, A, Weissbrich, C *et al.* (1990). Application of microbiological cancer test to cattle infected with bovine leucosis virus. *Arch Exp Veterinarmed* **44**: 205–212.
41. Horwitz, MS, Tufariello, J, Grunhaus, A and Fejer, G (1995). Model systems for studying the effects of adenovirus E3 genes on virulence in vivo. *Curr Top Microbiol Immunol* **199** (Pt 3): 195–211.
42. Wold, WS and Gooding, LR (1991). Region E3 of adenovirus: a cassette of genes involved in host immunosurveillance and virus-cell interactions. *Virology* **184**: 1–8.
43. Rawle, FC, Tollefson, AE, Wold, WS and Gooding, LR (1989). Mouse anti-adenovirus cytotoxic T lymphocytes. Inhibition of lysis by E3 gp19K but not E3 14.7K. *J Immunol* **143**: 2031–2037.
44. Feuerbach, D and Burgert, HG (1993). Novel proteins associated with MHC class I antigens in cells expressing the adenovirus protein E3/19K. *EMBO J* **12**: 3153–3161.
45. Beier, DC, Cox, JH, Vining, DR, Cresswell, P and Engelhard, VH (1994). Association of human class I MHC alleles with the adenovirus E3/19K protein. *J Immunol* **152**: 3862–3872.
46. Kaplan, JM, Armentano, D, Sparer, TE, Wynn, SG, Peterson, PA, Wadsworth, SC *et al.* (1997). Characterization of factors involved in modulating persistence of transgene expression from recombinant adenovirus in the mouse lung. *Hum Gene Ther* **8**: 45–56.
47. Reid, T, Galanis, E, Abbruzzese, J, Sze, D, Wein, LM, Andrews, J *et al.* (2002). Hepatic arterial infusion of a replication-selective oncolytic adenovirus (dl1520): phase II viral, immunologic, and clinical endpoints. *Cancer Res* **62**: 6070–6079.
48. Nemunaitis, J, Cunningham, C, Tong, AW, Post, L, Netto, G, Paulson, AS *et al.* (2003). Pilot trial of intravenous infusion of a replication-selective adenovirus (ONYX-015) in combination with chemotherapy or IL-2 treatment in refractory cancer patients. *Cancer Gene Ther* **10**: 341–352.
49. Heise, CC, Williams, A, Olesch, J and Kirn, DH (1999). Efficacy of a replication-competent adenovirus (ONYX-015) following intratumoral injection: intratumoral spread and distribution effects. *Cancer Gene Ther* **6**: 499–504.
50. Tong, AW, Nemunaitis, J, Su, D, Zhang, Y, Cunningham, C, Senzer, N *et al.* (2005). Intratumoral injection of INGN 241, a nonreplicating adenovector expressing the melanoma-differentiation associated gene-7 (mda-7/IL24): biologic outcome in advanced cancer patients. *Mol Ther* **11**: 160–172.